Electric Field-Induced Chemical Surface-Enhanced Raman Spectroscopy from Aligned Peptide Nanotube–Graphene Oxide Templates for Universal Trace Detection of Biomolecules

Sawsan Almohammed [a, b], Fengyuan Zhang [a, b], Brian J. Rodriguez * [a, b], and James H. Rice * [a]

[a]School of Physics, University College Dublin, Belfield, Dublin 4, Ireland
[b]Conway Institute of Biomolecular and Biomedical Research, University College Dublin, Belfield, Dublin 4, Ireland

Semiconductor–graphene oxide-based surface enhanced Raman spectroscopy substrates represent a new frontier in the field of surface enhanced Raman spectroscopy (SERS). However, the application of graphene oxide has had limited success due to the poor Raman enhancement factors achievable compared to noble metals. In this work, we report chemical SERS enhancement enabled by the application of electric field to aligned semiconducting peptide nanotube–graphene oxide composite structures during Raman measurements. The technique enables nanomolar detection sensitivity of glucose and nucleobases with up to 10-fold signal enhancement compared to metal-based substrates, which, to our knowledge, is higher than previously reported for semiconductor-based SERS substrates. The increased Raman scattering is assigned to enhanced charge-transfer resonance enabled by work function lowering of the peptide nanotubes. The substrate presented here is easy to make, low cost, sensitive, stable, highly reproducible, and can be used as an excellent platform for biomolecular sensing. These results provide insight into how semiconductor organic peptide nanotubes interact with graphene oxide, which may facilitate chemical biosensing, electronic devices, and energy harvesting applications.

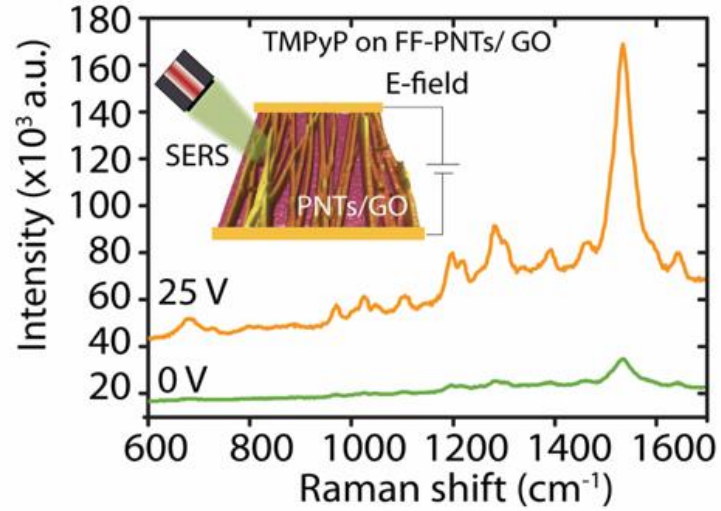

*e-mail correspondence to brian.rodriguez@ucd.ie and james.rice@ucd.ie

Introduction

Surface enhanced Raman spectroscopy (SERS) is a promising nondestructive analytical technique that enables single molecule detection with chemical specificity.[1–3] The most commonly used SERS substrates are nanostructured noble metals such as silver or gold. However, cost, stability, biological compatibility and environmental considerations have motivated the search for new SERS substrates.[4,5] Despite the fact that semiconductor-based SERS templates offer advantages in chemical stability and biocompatibility,[1–5] the enhancement factors are generally at least several orders of magnitude lower than those achieved using noble metals, thereby resulting in reduced detection sensitivity and limited practical application in areas such as biomedical analysis and diagnosis.[6–8] Up to now, a range of semiconductors have been employed for SERS, such as InAs/GaAs quantum dots,[6] CuTe nanocrystals,[7] Cu_2O nanospheres,[7] and TiO_2 nanostructures.[8] Wang et al. recently reported a ~ 10^5 SERS enhancement resulting from the creation of oxygen vacancies in semiconductor materials such as tungsten oxide, $W_{18}O_{49}$, which is the highest enhancement reported for a semiconductor-based SERS template.[1,2] 2D semiconducting graphene is another promising material for SERS that enhances Raman scattering.[9,10] Graphene oxide (GO) based materials are biocompatible,[1–5] thermally and chemically stable,[11] and can be produced at a high yield and low cost. However, relative to noble metals, GO is less effective at enhancing Raman scattering with Raman enhancement factors around 10^3 as opposed to ~ 10^{10}.[11–13] GO enhanced Raman scattering is generally attributed to the chemical contribution or chemical factor;[14–16] however, the mechanism is still under debate.[11–13] Several models have been put forward depending on the specific system under study, including metal-molecule charge transfer resonance.[11–16]

It has been previously reported that GO and semiconducting self-assembled diphenylalanine peptide nanotubes (FF-PNTs) form a nanocomposite through simple mixing.[9,10,17] The straightforward preparation of biocompatibile[18] self-assembled FF-PNTs[18] and specifically their piezoelectric and pyroelectric properties[19] and wide band gap[20] are attractive features of FF-PNTs and may facilitate charge transfer in combination with GO. As charge transfer depends on Fermi level alignment and internal fields (e.g., polarization of FF-PNT), it is reasonable to propose that an external electric field could potentially further enhance the SERS scattering efficiency thereby increasing the application range of graphene-based materials in SERS-based sensing[21,22] with further implications for energy harvesting,[23] drug delivery,[24] and other applications.[9,10,25] In this work, we employ FF-PNTs in combination with GO as an organic semiconducting SERS template and show that an externally applied electric field (from 5 to 25 V) can significantly increase the SERS enhancement factor by over an order of magnitude. This effect is attributed to enhanced charge-transfer resonance facilitated by field-induced lowering the work function of FF-PNTs. To demonstrate the potential of this technique, nanomolar detection of a range of biomolecules was undertaken including those with low Raman cross-sections such as glucose, thymine, lysine (lys), and bovine serum albumin (BSA). This detection sensitivity is on par with noble metals. In addition, the FF-PNT/GO template structure was found to be highly stable, reproducible and uniform. The demonstrated technique of using electric field during SERS measurements could also be applied to other semiconductor materials to improve SERS detection sensitivity.

Results and Discussion

Optical and Electrical Characterization of FF-PNT/GO Devices. Microfabricated aligned FF-PNT/GO nanocomposite substrates (shown schematically in Fig. 1(a)) were prepared on Si substrates. The gold electrodes were sputtered through openings in a 3D printed mask, as shown in Fig. S1, on Si substrates to achieve alignment.[26–28] The patterned regions were created by growing a silicon oxide layer (contact angle of 4.5 ± 1.2°) on a Si surface (contact angle of 68.3 ± 1.5°) via selective UV/ozone exposure. The difference in wettability between exposed and unexposed regions led to the alignment of the FF-PNT/GO structures during self-assembly (Fig. 1b, Figs. S1–S3). The density and alignment of the FF-PNTs increased with the addition of GO, as proved by SEM and AFM images (Figs. S3 and S4). The degree of alignment was determined (using a previously reported method)[26–28] from SEM images (Fig. S3) to be 5 ± 1° in comparison to 14 ± 1° for FF-PNTs only. The reduction in the degree of alignment is an indication of enhanced alignment.[26–28] These results in a good agreement with it has been reported in literature by which the addition of GO to FF-PNT, will lead to significantly improve the alignment of theses structure due to be attributed to the various amounts of hydrogen bonding and $\pi-\pi$ conjugation in FF-PNT/GO mixture composites.[29]

Conductivity measurements (Fig. S5) showed that the conductivity of the FF-PNTs increased with the addition of GO by ~ 36 %. Fourier transform infrared absorption spectroscopy showed no evidence that the incorporation of GO into the FF-PNTs altered the bonding structure of the FF-PNTs (Fig. S6). Optical absorption measurements showed (Fig. S7) that the band gap of FF-PNTs decreased from 5.20 eV to 5.04 eV in the presence of GO. Applying electric field on the composites (on a glass cover slip) resulted in further reduction of the band gap from 5.20 eV to 4.82 eV. A band gap reduction is a strong indication that the composite has become more electrically conductive,[9] in agreement with the increased conductivity (Fig. S5). Improved conductivity could be beneficial in sensing applications, specifically as a SERS-based sensor. Previous studies have shown that the presence of FF-PNTs could reduce the aggregation of GO during the drying process and facilitate the formation of an interweaving structure that could lead to good electron transfer kinetics. [9]

Electric Field-Induced SERS Enhancement. A greater than 10-fold increase in SERS intensity from meso-tetra (N-methyl-4-pyridyl) porphine tetrachloride (TMPyP) was obtained using the microfabricated FF-PNT/GO substrate in the presence of an applied electric field from 5 to 25 V/mm (Fig. 1c-f, and Fig. S8) using an excitation wavelength of 532 nm, which is in resonance with the Q band of TMPyP corresponding to an $e_g \leftarrow a_u$ electronic transition.[26–28] Notably, a greater than 30-fold increase in intensity for the 1573 cm^{-1} band (Fig. 1c) was observed. The increase in SERS intensity is accompanied with a lowering of the broad spectral background (Fig. 1f). Upon removal of the electric field the intensity returns to its original value over a ~ 60 minute period (Fig. 1e).

In contrast to when GO is combined with FF-PNTs, Raman spectroscopy studies of GO only (in the absence of FF-PNT) with TMPyP with an applied electric field showed a ~ 2-fold increase in Raman intensity between 10 – 25 V/mm (Fig. S9). While Raman spectroscopy for TMPyP on FF-PNTs only (in the absence of GO) produces a ~ 3 to 4-fold increase in SERS Intensity at an electric field between 10 – 25 V/mm (Fig. S9). In all cases, the Raman intensity decreases at an electric field of ~ 30 – 60 V/mm.

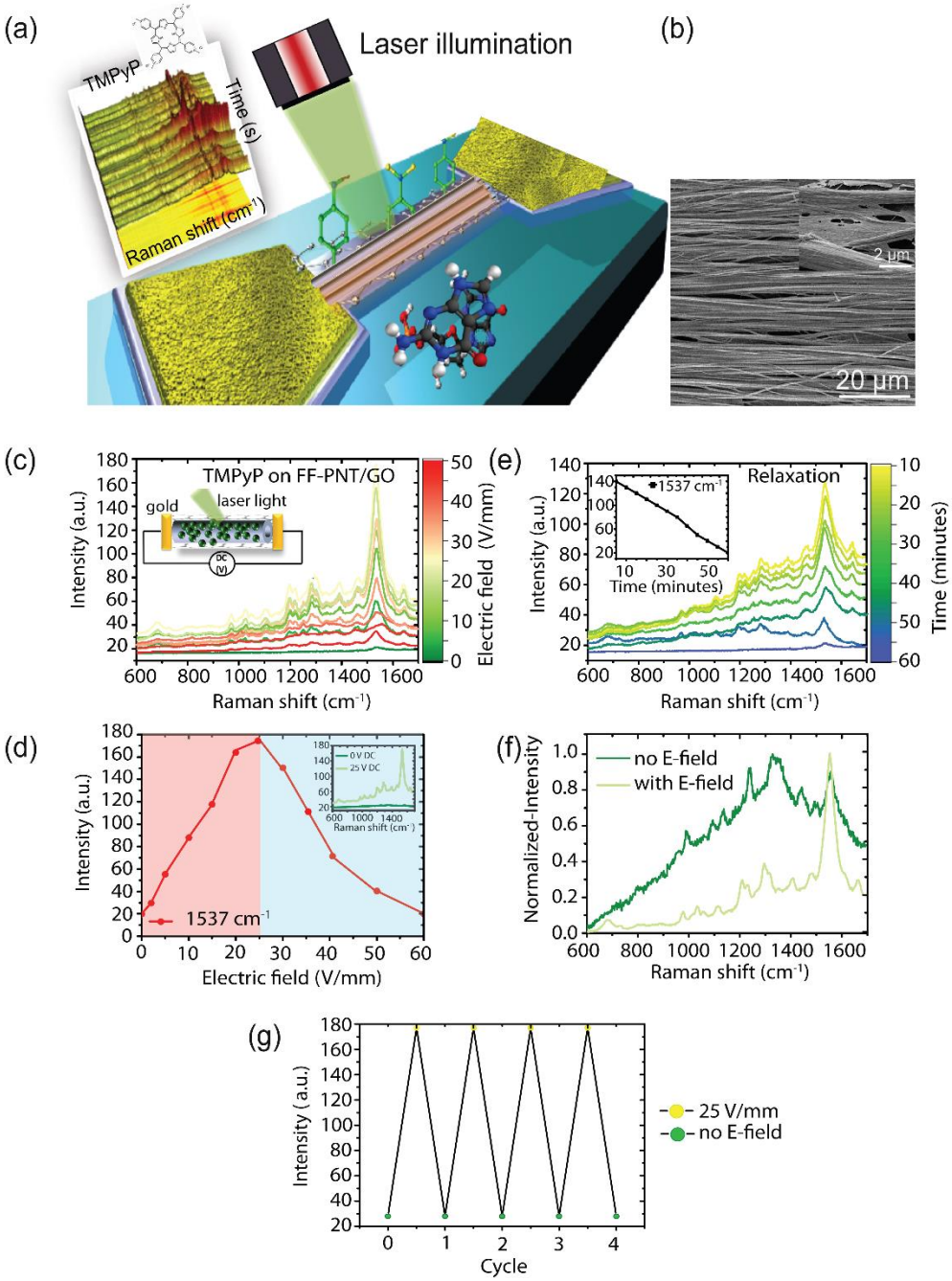

Figure 1. (a) Schematic illustration of the substrate design used in the study. The inset in **(a)** shows Raman spectra from the analyte molecule TMPyP at a relatively low concentration of ~ 10^{-11} M on FF-PNT/GO template with an applied electric field of 25 V/mm. **(b)** SEM image of the FF-PNT/GO substrate and **(c-f)** SERS spectra from TMPyP probe molecules on FF-PNT/GO on Si at electric field applied from 0 – 50 or 60 V/mm. **(c)** SERS spectra recorded with electric field. **(d)** Plot of SERS intensity versus electric field applied. The inset in (**d**) shows a comparison of normalized SERS spectra at 0 V/mm and 25 V/mm. **(e)** SERS Raman signal intensity with relaxation time. The inset shows plot of the relative intensity of TMPyP bands at 1537 cm^{-1} as a function of the relaxation time. **(f)** Normalized SERS spectra recorded at 0 and 25 V/mm. **(g)** plot of SERS intensity at electric field of 20 V/mm in comparison with no electric field at different cycle. The red shading corresponds to the area from which maximum SERS can be seen (5 – 25 V/mm). The blue shading indicates the regime where a reduction in SERS can be seen at electric field values (30 – 60 V/mm).

Plotting applied electric field strength against Raman signal strength showed that there was an optimum field strength (25 V/mm) that achieved the strongest Raman intensity in FF-PNT/GO template, which if exceeded resulted in reduced Raman signal (Fig. 1d). When applying a field of 30 V/mm, the Raman signal intensity dropped ~ 12 %, while an applied electric field of 60 V/mm resulted in a ~ 89 % reduction in Raman signal intensity. Similar results were recorded from other dye molecules such as rhodamine B (RhB) and methylene blue (MB) (Fig. S10). An increase in SERS intensity was observed from both using electric field between 10 – 25 V/mm, combined with strong quenching in the fluorescence background in comparison with the absence of applied electric field, indicating possible charge transfer in the system. Previous studies have shown that on a GO-based substrate, RhB interacts with GO through the aromatic rings. The long axis of the RhB molecules should be approximately parallel to the layer of GO due to strong π–π stacking, which induces charge transfer between the RhB and GO and is responsible for the strong Raman signal enhancement and the quenching of fluorescence.[11–13,30–32]

The reduction in the Raman intensity when electric field exceed 25 V/mm could be associated with FF-PNT pyroelectricity. FF-PNTs are known to exhibit both piezo-[22,23] and pyroelectric[19] properties.[30–34] These effects might be activated by applying the electric field and excess electrons might enhance and promote the charge transfer processes between the FF-PNTs and GO and hence enhance SERS from the analyte.[9,10,21, 22,27–29] Previous studies have shown that the pyroelectric effect exhibited by the FF-PNTs reduces as the temperature increases beyond 55 °C.[19] This effect may explain why the SERS intensity in our case dropped at electric fields between 30 – 60 V/mm, for which the substrate heats up to 60 – 100 °C, respectively. For this reason, heat generated from the substrate was measured to determine the heat produced. The FF-PNT/GO template was determined to heat up when an electric field was applied. Applying an electric field of 10 – 60 V/mm resulted in temperature increases from 40 °C (at 10 V/mm) to 110 °C (at 60 V/mm) (Fig. S11). An increase in SERS intensity was recorded with an electric field range from 10 – 25 V/mm (Fig. 1), the substrates temperature at these field strengths ranging between 40 – 55 °C for 10 – 25 V/mm, respectively. The SERS signal intensity decreasing as the applied field increases from 30 – 60 V/mm, at these field strengths the substrate has a temperature range from 60 – 100 °C, for 30 – 60 V/mm, respectively.

This indicates that a pyroelectric-related effect may contribute to the observed SERS signal increase or decrease with applied electric field. To make these observations more concrete, UV irradiation (λ = 254 nm) was introduced into FF-PNT/GO TMPyP system. This irradiation wavelength corresponds to super band gap excitation of the FF-PNTs, resulting in the formation of electron-hole pairs (Fig. S12). UV irradiation of the FF-PNT/GO system (Fig. S12) resulted in a significant (~ 10^7 to 10^8) increase in SERS intensity, which is comparable to the results recoded using Ag NP/FF-PNT system, as reported previously.[18] Relaxation or recovery of the SERS signal to its original intensity was recoded over ~ 60 minutes upon the removal of UV irradiation.

Reversible Control of Raman Signal Intensity. Reversible control over the precise Raman signal intensity can be easily achieved by controlling the electric field strength. Returning the electric field from high field strengths (e.g., > 25 V/mm) to low fields (e.g., < 25 V/mm) resulted in increased SERS intensity, demonstrating reversible tuning of the SERS signal intensities with applied electric field (Fig. S13). Stability and reproducibility tests were performed on the FF-

PNT/GO template. SERS signal intensity varied < 5 % (Fig. S13). These results demonstrate that the FF-PNT/GO template is highly uniform and stable under an applied field.[11–13] The uniformity of the SERS signals collected from randomly selected positions over the template or different samples were performed (Fig. S14). A change of ~ 3 – 4 % was observed for electric fields between 20 and 30 V/mm; fields between 40 and 60 V/mm resulted in SERS intensity variations of ~ 10 – 20 % (Fig. S14).

One possible explanation for the large increase in SERS intensity with applied electric field on the FF-PNT/GO template is that the electric field induces reorientation through vibrational and rotational motions of the probe molecule. This resulting in changes of the polarizability and dipole momentum of the probe molecule until the system reaches equilibrium resulting in an increased Raman scattering cross section resulting in an increased SERS signal intensity.[35–37] Additionally, FF-PNTs are well known to have both piezo-[22,23] and pyroelectric[19] properties, these effects might be activated by applying the electric field which might induce vibrational and heating of the tubes (Fig. S11 and S12), as discussed above. Once the tubes vibrate or heat up more electrons or charge can be produced. Potentially these excess electrons enhance and promote the charge transfer processes between the FF-PNTs and GO and hence enhance SERS intensity from the analyte.[9,10,21,22,27–29]

Charge-Transfer Processes. In order to better understand the mechanism for the observed increased in Raman intensity on FF-PNT/GO template with applied electric field, studies where undertaken using the probe molecule 4-aminobenzenethiol (4-ABT). 4-ABT can form a charge transfer complex with semiconductors such as zinc oxide, resulting in an increase in selected Raman band intensities.[38]

The SERS spectrum recorded for 4-ABT on the FF-PNT/GO substrate template prior to applying an electric field shows (Fig. 2a,b and Fig. S15) only vibrational modes with a_1 symmetry at 1088, and 1594 cm^{-1} which are assigned to the Raman spectrum of the 4-ABT in the literature.[39,40] Through the application of an electric field of increasing strength the Raman spectral features change (Fig. 2a and Fig. S15) with b_2 mode bands (1432, 1390, 1144, and 1076 cm^{-1}) progressively appearing with increasing electric field from 5 to 25 V/mm. The 4-ABT Raman b_2 modes are reported to be enhanced through a charge transfer effect, in our case we could observe these bands without the need for metal nanoparticles, only by using semiconductor FF-PNT/GO. This potentially achieved through a charge transfer-based effect that is enhanced by applying electric field that results in the activation of piezoelectric FF-PNT by allowing the generation of more electrons that undergo charge transfer.

Previous studies have shown [9,10,21,22] that charge transfer processes are possible between FF-PNTs and GO as the work function of FF-PNT is around ~ 5.1 eV (determined from Fig. 3e) while the work function of GO is 4.9 eV (as indicated in Fig. 2e).[9,10,21,22,27–29] The difference between the Fermi level of the aligned FF-PNTs and graphene oxide is ~ 0.2 eV, which is less than the laser excitation (532 nm; 2.3 eV). It is possible that the energy of the Raman excitation laser can facilitate the transfer of charge from FF-PNTs to GO. The lowest unoccupied molecular orbital (LUMO) of 4-ABT (Fig. 2e) is located 4.0 eV below the vacuum level.[28,39,40] The difference between the Fermi level of the aligned FF-PNTs and the LUMO is ~ 1.1 eV, which is less than the laser excitation (532 nm; 2.3 eV). Therefore, it is possible that the excitation facilitates charge transfer from the aligned FF-PNT/GO template to 4-ABT.

SERS with electric field (from 0 – 25 V) of 4-ABT at concentrations as low as nanomolar were recorded (Fig. 2c). At this low probe molecule concentration SERS Raman intensity fluctuations were observed. Such blinking in SERS intensity is associated with few/single molecule detection that could be as a results of charge transfer process. An optimum electric field strength (e.g., 25 V/mm) was found thereafter a decline in Raman intensity was observed (Fig. 2d), as with the previous probe molecule (Fig. 1d). Removal of the electric field results in a return to the original Raman spectrum seen before the field was applied demonstrating that the process in fully reversible (Fig. S15). After relaxation and by applying electric field again from 5 to 25 V/mm, the appearance of intense b_2 Raman bands can again be seen, showing that the substrate exhibits fully reversible behavior (Fig. S15).

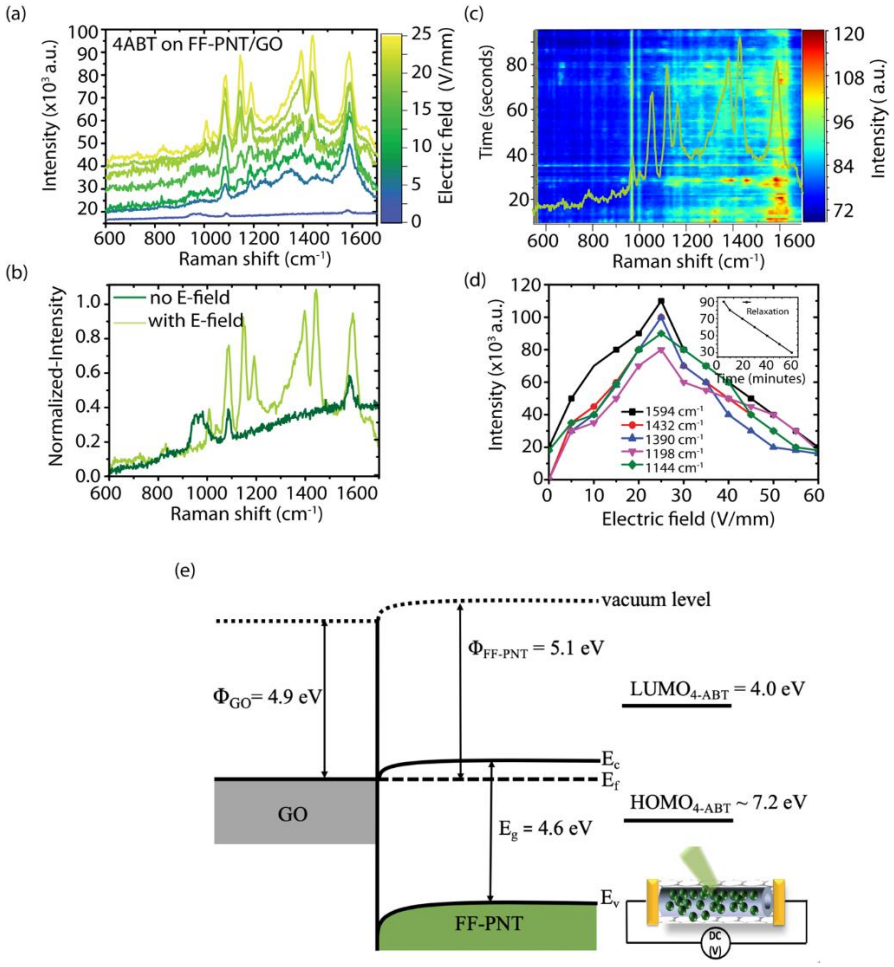

Figure 2. (a-d) SERS spectra from 4-ABT probe molecules on FF-PNT/GO on Si. **(a)** SERS spectra recorded with electric field from 0 – 25 V/mm. **(b)** Comparison of normalized SERS spectra recorded with electric field at 25 V/mm and at 0 V/mm. **(c)** SERS recorded for 4-ABT, were the concentration of the probe molecule was nanomolar. The spectra recorded as a time sequence over 100 s. **(d)** Plot shows the relative intensity changes with applied electric field from 0 – 60 V/mm. The inset shows relaxation of the signal intensity after removing the electric field over period of ~ 60 minutes. **(e)** Band energy diagram of the FF-PNT/GO junction where Φ is the work function, E_f is the Fermi level, E_c is the conduction band, and E_v is the valance band. The highest occupied molecular orbital (HOMO) of 4-ABT is located 7.18 eV below the vacuum level while the lowest unoccupied molecular orbital (LUMO) is located 4.0 eV below the vacuum level.

SERS recorded with only GO with 4-ABT (in the absence of FF-PNTs), results in only the detection of GO bands, and no appearance of 4-ABT Raman bands can be seen (Fig. S16). These results further prove the advantage of having FF-PNTs as a template to enhance chemical enhancement in SERS that facilities the detection of non-resonant molecules at low concentrations.

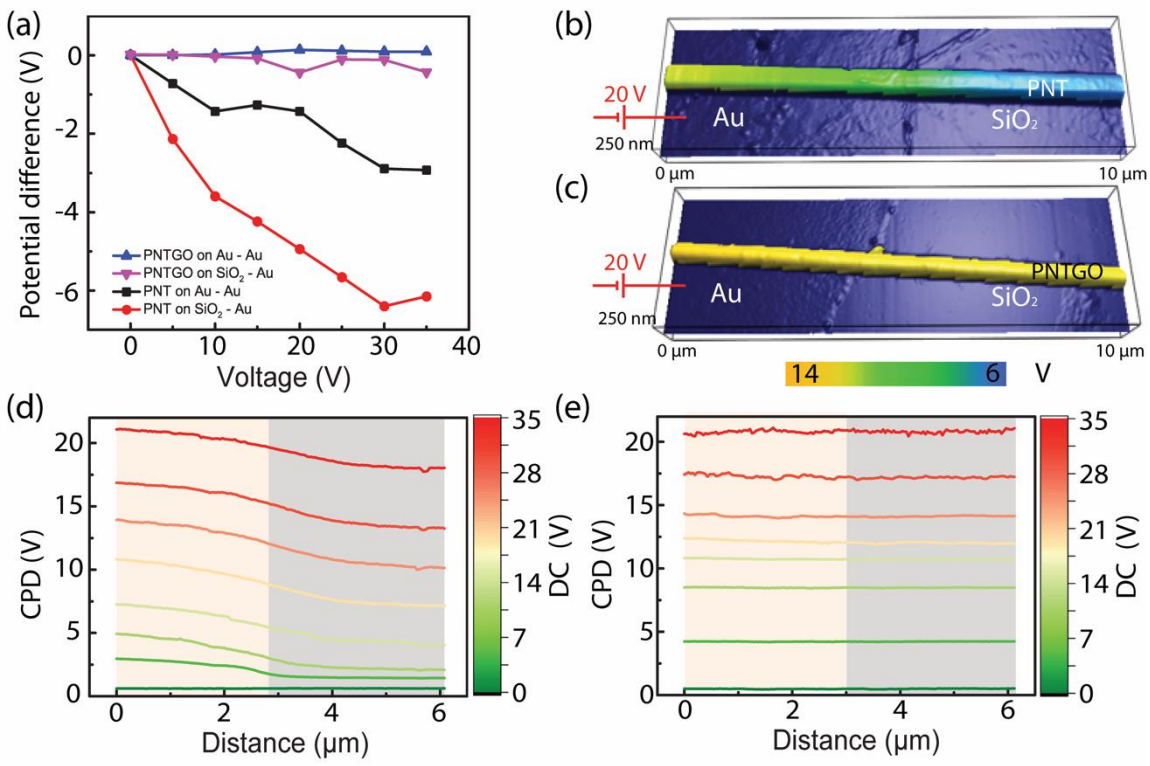

Figure 3. Kelvin probe force microscopy (KPFM) measurements performed on both FF-PNT and FF-PNT/GO at the edge of a biased Au electrode on the SiO_2–Si substrate. **(a)** Potential difference between FF-PNT (on Au and SiO_2 regions) and Au electrode and between FF-PNT/GO (on Au and SiO_2 regions) and Au electrode. Each point is the mean value for potential difference calculated from the same 1 μm^2 area and each point in the same line is determined from the same position. The potential differences on SiO_2 are calculated 2 µm away from the edge of the Au. Three dimensional topographical images of **(b)** FF-PNT and (c) FF-PNT/GO with CPD (contact potential difference) superimposed only on the tubes for a voltage of 20 V applied to the Au electrode. The color bar from yellow to light blue indicates the CPD value. CPD on a line profile on the FF-PNT **(d)** and FF-PNT/GO **(e)** in **(b, c),** respectively. Different colors indicate different applied dc voltage on gold electrode. The applied voltage starts from 0 – 35 V with a 5 V step. The light orange color **(d, e)** in the background indicates the FF-PNT **(b)** and FF-PNT/GO **(c)** on Au area while the light gray color **(d, e)** indicates the FF-PNT **(b)** and FF-PNT/GO **(c)** on SiO_2 area.

To give further insight into the influence of applied electric field on the FF-PNT/GO template and the possible charge transfer in the system, SERS measurements were performed in the absence of the probe molecule (Figs. S17 and S18). The spectra show evidence of changes in the Fermi level of GO through changes in relative band intensities for the G- and D-bands with applied voltage (Fig. S18b, and c). The applied electric field potentially modulates the energy

alignment between the HOMO/LUMO of the probe molecule and the Fermi level of G, driving the entire system in and out of charge transfer resonance. Before the electric field is applied, the energy difference between the Fermi level of GO and 4-ABTs LUMO is of the order < 1 eV (Fig. 2e), with the applied electric field potentially reducing this difference in energy resulting in more efficient charge transfer. Noting that too high an electric field then drives out of resonance the energy levels decreasing charge transfer efficiency. Kelvin probe force microscopy (KPFM) measurements revealed that in the presence of GO an FF-PNT connected to a biased electrode remained at the same potential even several microns away from the electrode. In the absence of GO, the potential decreased along the -FFPNT (Fig. 3). This further confirms that the FF-PNT/GO substrate is conducting over the entire tube length. This enables the charge to move to a site near/at a GO site for charge transfer. The composite structure of the FF-PNT/GO template was found to be highly stable after the application of electric field between 5 and 60 V/mm, as evidenced by SEM images in Fig. S19 and Energy dispersive X-Ray spectroscopy (EDX) mapping Fig. S20.

Biomolecular Sensing. To further demonstrate the methodology, analysis of biochemical molecules was undertaken. Glucose is an important biomolecule that needs to be monitored in patients with diabetes with glucose levels in saliva being in the range 50 – 500 µM.[41,42] The ability to detect glucose at these levels with high signal to noise ratios is attractive in order to design minimally invasive methods for frequent glucose monitoring. The spectral methodology was applied to enhance the SERS signal from glucose at a concentration of 10 µM (Fig. 4a, Fig. S21). Following the application of an electric field from 5 – 25 V/mm, there was significant (~ 10-fold increase in intensity for band at 1185 cm^{-1}) enhancement in SERS signal in comparison with SERS spectra recorded in the absence of electric field. This study shows that when an electric field is applied, the template can detect glucose at levels required for medical diagnostics.

SERS investigations of thymine were also undertaken (Fig. 4b and Fig. S21). The study of this molecule provides insight into how DNA interacts with the substrate – information of potential interest in the development of DNA/RNA assays. SERS of thymine increase (~ 10-fold) signal intensity with optimum electric field strength with thymine detected at a concentration of ~ 1 nM (Fig. S22). The spectra show clear evidence of blinking with large variations in Raman peak intensities and positions over time. While these peaks differ in frequency, relative intensities, and line-width, they can all be assigned to vibrational bands of thymine[43,44] as the average SERS signal is constant with the Raman spectra of the probe molecule at a higher concentration (Fig. 4).

Proteins BSA and lysine were also studied and showed significant SERS signal enhancement (~ 10-fold increase in SERS signal (Figs. 4c,d and S23); all bands detected are in a good agreement with literature values).[45–50] These molecules are commonly used in biomedical assays and the results show the potential applicability of the FF-PNT/GO substrates to medical assay technology. Another molecule of interest in the pharmaceutical industry is nitrophenol (4-NIP) and its derivatives. It is well known that they may cause damage to the central nervous system, liver, kidney, and both animal and human blood.[51] Therefore, detection of 4-NIP in the environment is of great interest. Applying the optimum field strength resulted in a ~ 9-fold increase in SERS intensity, accompanied with detection of all 4-NIP bands (Fig. 4e). Raman bands at 1440, 1500, and 1580 cm^{-1} are the vibrational modes of the molecule. The band at

1330 cm^{-1} is assigned to the symmetric stretching mode of the nitro group in agreement with literature.[51] The SERS signal reduced for fields in the range of 30 – 60 V/mm.

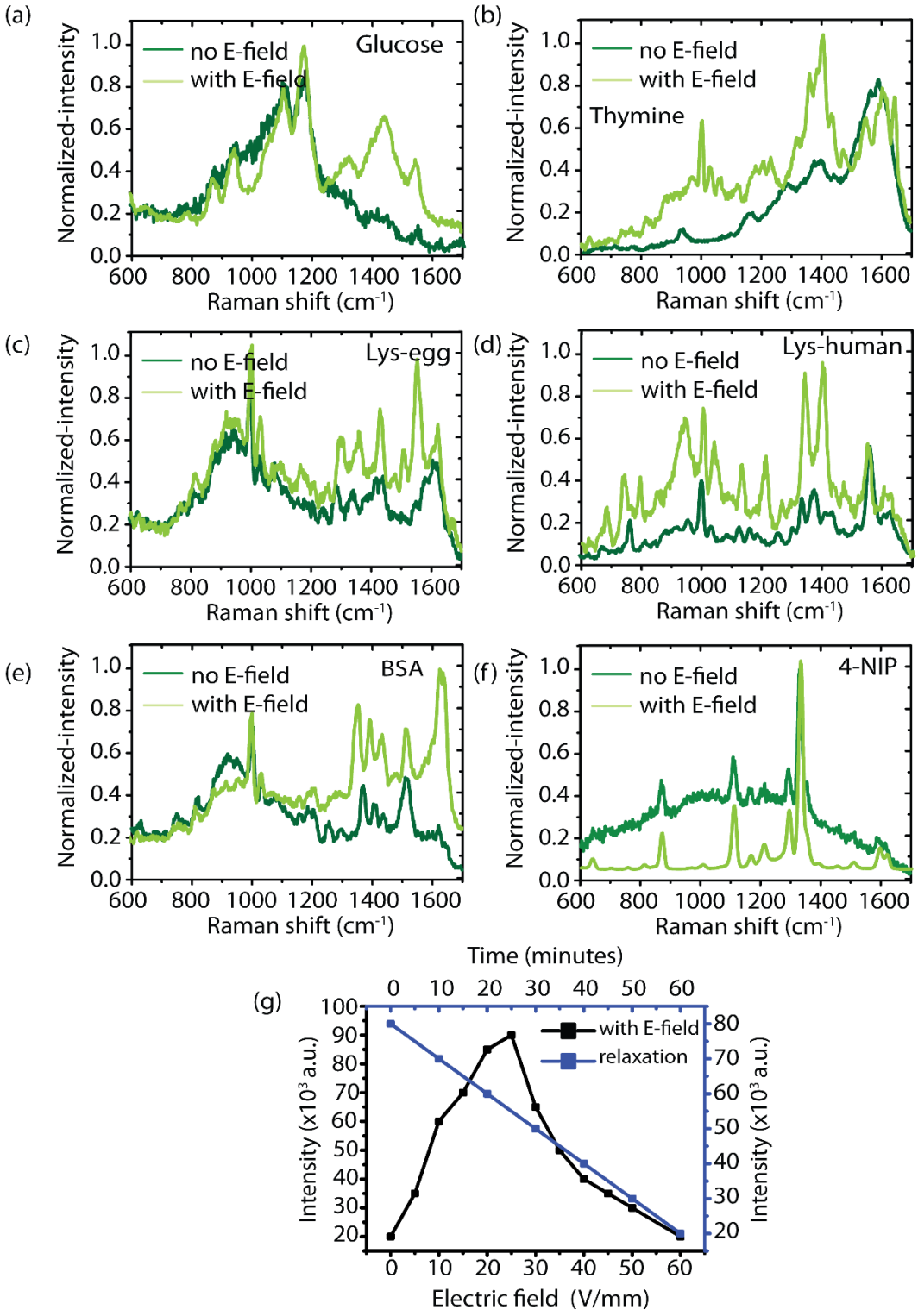

Figure 4. SERS spectra for a series of probe molecules on FF-PNT/GO template at electric field of 25 V/mm versus SERS spectra with no electric field applied. Concentration of the probe molecules was 10 µM. **(a)** Glucose, **(b)** thymine, **(c)** lysine from egg, **(d)** lysine from human, **(e)** bovine serum albumin (BSA), and **(e)** nitrophenol (4-NIP). **(g)** Plot of electric field versus SERS intensity (for lys) shows relaxation of the intensity over a period of 60 minutes.

Combining semiconducting GO with organic self-assembling piezoelectric semiconducting peptide nanotubes (FF-PNT) and applied external electrical fields gives rise to an order of magnitude SERS signal enhancement for a wide range of small molecules. The increase in SERS intensity is attributed to enhancement in the SERS chemical factor that can be tuned with applied electric field in the 5 – 25 V/mm range, allowing the detection of molecules at concentrations as low as nanomolar. The ability to detect a variety of molecules can lead to a wide range of applications for the aligned FF-PNT/GO template, such as chemical sensors. This work provides a promising strategy and platform towards the design of SERS devices for achieving a highly sensitive portable tool for molecular sensing for various applications, such as food safety, glucose monitoring, medical diagnostics, or in electronic devices and energy harvesting applications. The demonstrated technique of using electric field during SERS measurements could potentially be applied to other semiconductor materials to improve sensitivity.

Experimental Details

Preparation of FF-PNT solution

FF-PNTs were prepared by dissolving the L-diphenylalanine peptide (Bachem, Bubendorf, Switzerland) in 1,1,1,3,3,3-hexafluoro-2-propanol (Sigma-Aldrich, Ireland) at an initial concentration of 100 mg/ml, which was then further diluted in deionized water to a final concentration of 2 mg/ml for FF-PNTs to self-assemble. Fresh stock solutions were prepared for each experiment.

Preparation of GO solution

Single layer graphene oxide (SLGO, cheap tubes USA). Dimension from AFM from 300 – 800 nm lateral dimension with 1 – 2 nm thick. Graphene was prepared by dissolving graphene powder ~ 1 g in dH_2O (100 ml) to final concentration of 2 mg/ml then further diluted to 1 mg/ml and 0.5 mg/ml in dH_2O too.

Preparation of Si substrate with gold electrode

Si wafers (Si Mat), cut to 2 cm x 1 cm, were cleaned of surface contaminants by dipping in acetone for 2 minutes and then washed with ethanol and isopropanol (Sigma-Aldrich). De-ionized water was used to rinse the substrates, which were then blown dry using nitrogen. To fabricate interdigitated gold electrode pairs on the Si substrate, gold was sputtered through mask openings in a 3D printed mask with dimensions of 2 cm x 1 cm and opening ~ 0.1 mm. In order to create a patterned region, a mask with one opening of 1 mm, was placed above the gold electrode.

Preparation of FF-PNT/GO template

FF-PNT/Ag NP templates were prepared using 2 mg/ml of FF solution heated at 100 °C for 2 minutes and GO at different concentrations 2, or 1, and 0.5 mg/ml. 40 µl of GO solution was added to 60 µl of the heated FF solution and stirred for 3 minutes. 30 µl of the mixed solution was then deposited on the patterned Si substrate with interdigit electrodes to create the aligned FF-PNT/GO template.

Preparation of probe molecule solutions

To prepare meso-tetra (N-methyl-4-pyridyl) porphine tetrachloride (TMPyP) (T40125, Frontier Scientific) solutions, TMPyP powder was diluted with deionized water to a final

concentration of 10^{-4} M. The solution was further diluted with deionized water to a range of concentrations, from 10^{-5}–10^{-7} M. Similarly, with rhodamine B (RhB) (R6626-25G, Sigma-Aldrich Ireland), glucose (49163, Sigma-Aldrich Ireland), thymine and methylene blue (MB) (Sigma-Aldrich Ireland M9140), bovine serum albumin (BSA), lys-egg and lys-human (albumin from chicken egg white and humans, respectively) all sourced from Sigma-Aldrich Ireland. 4-aminothiophenol (PATP) or 4-ABT (CAS 1193-02-8, New Star Chemical) solution was prepared by dissolving PATP powder in methanol to a concentration of 10^{-4} M. The solution was then further diluted with deionized water to lower concentrations of 10^{-5} or 10^{-6} M. 4-Nitrophenol solution (N7660, Sigma-Aldrich Ireland) was diluted with deionized water to a final concentration of 10^{-4} M or 10^{-6} M.

UV-vis absorbance spectrometer

Optical absorbance measurements of FF-PNTs with and without Ag NPs and the analyte molecule PATP and 2-AMP were performed on an UV-vis absorbance spectrometer (V-650, JASCO, Inc.) under identical settings: 1 nm step size, 1 nm bandwidth, and 400 nm/minute scan speed across a 190-900 nm range. A quartz cuvette or glass cover slip was used to conduct the measurements.

Fourier transform infrared spectroscopy

FTIR measurements were performed using Alpha. Platinum-ATR (12209186, Bruker). A small drop of FF-PNT (10 µl) was placed on the ATR diamond crystal. The spectrum was collected using transmission mode scanning from 1400 – 4000 nm.

Scanning electron microscopy (SEM)

SEM (JSM-7600F, JEOL, operated at 5 kV) was employed to characterize and observe the location of NPs decorating the surface. A thin (~ 8 nm) layer of gold was sputtered on the samples before SEM imaging (Hummer IV, Anatech USA).

Kelvin probe force microscopy (KPFM)

KPFM was performed using an atomic force microscope (AFM) (MFP-3D, Asylum Research) and a voltage amplifier (F10A, FLC Electronics AB). An asyelec-01 tip (Asylum Research) with Ir coating was used to measure the contact potential difference (CPD) between the tip and sample surface. KPFM images were measured at the edge of a biased Au electrode on a SiO_2 on Si substrate with a lift height of 50 nm. The dc bias applied to the Au electrode was varied from 0 – 35 V.

Raman spectroscopy

SERS measurements were performed using a bespoke Raman system that consisted of an inverted optical microscope (IX71, Olympus), a monochromatic laser (Green laser, ThorLabs) with beam splitter and long pass filter (RazorEdge, Semrock), a spectrograph (SP-2300i, Princeton Instruments), and a CCD camera (IXON, Andor). To focus the laser (532 nm wavelength, 5 mW incident power), a 50x objective was used. Raman spectra were collected with an exposure time of 1 s. 30 µl of the analyte molecule TMPyP or RhB or Glucose at concentration of 10^{-5} M, 10^{-7} or 10^{-9} M was deposited above the aligned FF-PNTs in the presence and absence GO. The average of typically 10 measurements, is reported. Toluene was used for calibration of the Raman signal over the spectral window. SERS measurements were performed during in situ applied electric field from 0 – 60 V/mm, in step of 5 V/mm. UV

irradiation (using a UV lamp with a wavelength of 254 nm and a nominal output power of 4.5 mW/cm^2 (40-759, Edmond Optics) was used to conduct the measurement on FF-PNT/GO with TMPyP, at period of around 20 – 45 minutes at 2.2 cm for TMPyP. Relaxation was also recoded after removing the applied electric field (~ 60 min) or by applying low electric field values. The heat generated from the substrate during the application of electric field was measured using a voltmeter (TENMA-727725) with thermocouple sensor placed in contact with the sample.

Acknowledgements

This research was funded by the Ministry of Higher Education of Saudi Arabia under the King Abdullah Scholarship Program (ref. no. IR10161), the China Scholarship Council, the European Union's Horizon 2020 research and innovation program under Marie Skłodowska-Curie grant agreement number 644175, and Science Foundation Ireland (12/IP/1556, 07/IN1/B931, 14/US/I3113, SFI/17/CDA/4637). The authors acknowledge Ian Reid for assistance with SEM, and Gareth Redmond for access to UV-vis, and Aaron Martin for access to FTIR. The authors acknowledge Michael McDermott and Jim McDaid of the School of Physics for assistance with temperature measurements. The authors also acknowledge Jose Lopez for 3D printing the mask used to prepare the interdigitated electrodes (Enterprise Ireland (CF-2016-0389-P)) and Sebastian Tadeusz Barwich for assistance with IV measurements.

Author contributions

S.A., B.R., and J.R. designed the experiments and developed the experimental set-up. S.A. carried out sample preparation and Raman, FTIR, UV-vis, PL and SEM measurements. F.Z. performed AFM measurements. All authors analyzed data, discussed results, and wrote and reviewed the manuscript.

References

(1) Cong, S.; Yuan, Y.; Chen, Z.; Hou, J.; Yang, M.; Su, Y.; Zhang, Y.; Li, L.; Li, Q.; Geng, F.; et al. Noble Metal-Comparable SERS Enhancement from Semiconducting Metal Oxides by Making Oxygen Vacancies. *Nature Communications* **2015**, *6*, 7800.

(2) Zheng, Z.; Cong, S.; Gong, W.; Xuan, J.; Li, G.; Lu, W.; Geng, F.; Zhao, Z. Semiconductor SERS Enhancement Enabled by Oxygen Incorporation. *Nature Communications* **2017**, *8* (1), 1–11.

(3) Han, X. X.; Ji, W.; Zhao, B.; Ozaki, Y. Semiconductor-Enhanced Raman Scattering: Active Nanomaterials and Applications. *Nanoscale* **2017**, *9* (15), 4847–4861.

(4) Qu, S.; Liu, H.; Dong, L.; Wu, L.; Ma, C.; Wang, S. Graphene-Hexagonal Boron Nitride Heterostructure as a Tunable Phonon–Plasmon Coupling System. *Crystals* **2017**, *7* (2), 49.

(5) Zhang, X.; Si, S.; Zhang, X.; Wu, W.; Xiao, X.; Jiang, C. Improved Thermal Stability of Graphene-Veiled Noble Metal Nanoarrays as Recyclable SERS Substrates. *ACS Appl. Mater. Interfaces* **2017**, *9* (46), 40726–40733.

(6) Song, H.; Li, X.; Yoo, S.; Wu, Y.; Liu, W.; Wang, X.; Liu, H. Highly Sensitive Surface-Enhanced Raman Spectroscopy from Ag Nanoparticles Decorated Graphene Sheet. *J. Nanomater.* **2014**, *2014,* 1–7.

(7) Li, Y.; Li, Z.; Chi, C.; Shan, H.; Zheng, L.; Fang, Z. Plasmonics of 2D Nanomaterials:

Properties and Applications. *Adv. Sci.* **2017**, *4* (8), 1–25.
(8) Deng, H.; Zhang, X.; Wu, W.; Wang, F.; Si, S.; Zhang, X.; Jiang, C.; Xiao, X.; Dai, Z. Mercuric Contamination: Ultrasensitive SERS Substrate Integrated with Uniform Subnanometer Scale "Hot Spots" Created by a Graphene Spacer for the Detection of Mercury Ions. *Small* **2017**, *13* (9), 2017.
(9) Ivanov, M. S.; Khomchenko, V. A.; Salimian, M.; Kopyl, S.; Buryakov, A. M. Self-Assembled Diphenylalanine Peptide Microtubes Covered by Reduced Graphene Oxide / Spiky Nickel Nanocomposite : An Integrated Nanobiomaterial for Multifunctional Applications. *Materials & Design* **2018**, *142*, 149–157.
(10) Yilmaz, M.; Babur, E.; Ozdemir, M.; Gieseking, R. L.; Dede, Y.; Tamer, U.; Schatz, G. C.; Facchetti, A.; Usta, H.; Demirel, G. Nanostructured Organic Semiconductor Films for Molecular Detection with Surface-Enhanced Raman Spectroscopy. *Nature Materials* **2017**, *16* (9), 918–924.
(11) de Abajo, F. J. G. Graphene Plasmonics: Challenges and Opportunities. *ACS Photonics* **2014**, *24*, 135–152.
(12) Goul, R.; Das, S.; Liu, Q.; Xin, M.; Lu, R.; Hui, R.; Wu, J. Z. Quantitative Analysis of Surface Enhanced Raman Spectroscopy of Rhodamine 6G Using a Composite Graphene and Plasmonic Au Nanoparticle Substrate. *Carbon* **2017**, *111*, 386–392.
(13) Lu, R.; Konzelmann, A.; Xu, F.; Gong, Y.; Liu, J.; Liu, Q.; Xin, M.; Hui, R.; Wu, J. Z. High Sensitivity Surface Enhanced Raman Spectroscopy of R6G on in Situ Fabricated Au Nanoparticle/Graphene Plasmonic Substrates. *Carbon* **2015**, *86*, 78–85.
(14) Xu, H.; Xie, L.; Zhang, H.; Zhang, J. Effect of Graphene Fermi Level on the Raman Scattering Intensity of Molecules on Graphene. *ACS Nano* **2011**, 5, 5338–5344.
(15) Yu, Y.J.; Zhao, Y.; Ryu, S.; Brus, L. E.; Kim, K. S.; Kim, P. Tuning the Graphene Work Function by Electric Field Effect. *Nano Letters* **2009**, *9* (10), 3430–3434.
(16) Balu, R.; Zhong, X.; Pandey, R.; Karna, S. P. Effect of Electric Field on the Band Structure of Graphene/Boron Nitride and Boron Nitride/Boron Nitride Bilayers. *Applied Physics Letters* **2012**, *100* (5), 1–4.
(17) Bhattacharya, A.; Cheng, J.; Bhosale, S.; Aphale, A.; Patra, P. K.; Mukerji, I. UV Resonance Raman Characterization of Diphenylalanine – Graphene. *Spectroscopy* **2012**, *27*, 2–8.
(18) Reches, M.; Gazit, E. Controlled Patterning of Aligned Self-Assembled Peptide Nanotubes. *Nature Nanotechnology* **2006**, *1*, 195–200.
(19) Esin, A.; Baturin, I.; Nikitin, T.; Vasilev, S.; Salehli, F.; Shur, V. Y.; Kholkin, A. L. Pyroelectric Effect and Polarization Instability in Self-Assembled Diphenylalanine Microtubes. *Applied Physics Letters* **2016**, *109* (14), 1–5.
(20) Takahashi, R.; Wang, H.; Lewis, J. P. Electronic Structures and Conductivity in Peptide Nanotubes. *Journal of Physical Chemistry B* **2007**, *111* (30), 9093–9098.
(21) Wang, Z.; Huang, P.; Bhirde, A.; Jin, A.; Ma, Y.; Niu, G.; Neamati, N.; Chen, X. A Nanoscale Graphene Oxide–Peptide Biosensor for Real-Time Specific Biomarker Detection on the Cell Surface. *Chemical Communications* **2012**, *48* (78), 9768.
(22) Li, Q.; Liu, L.; Zhang, S.; Xu, M.; Wang, X.; Wang, C.; Besenbacher, F.; Dong, M. Modulating Aβ33-42 Peptide Assembly by Graphene Oxide. *Chemistry - A European Journal* **2014**, *20* (24), 7236–7240.
(23) Nguyen, V.; Jenkins, K.; Yang, R. Epitaxial Growth of Vertically Aligned Piezoelectric Diphenylalanine Peptide Microrods with Uniform Polarization. *Nano Energy* **2015**, *17*, 323–329.

(24) Silva, R. F.; Araújo, D. R.; Silva, E. R.; Ando, R. a.; Alves, W. a. L -Diphenylalanine Microtubes as a Potential Drug-Delivery System: Characterization, Release Kinetics, and Cytotoxicity. *Langmuir* **2013**, *29*, 10205–10212.
(25) Tao, K.; Makam, P.; Aizen, R.; Gazit, E. Self-Assembling Peptide Semiconductors. *Materials Science* **2017**, *885*, 358.
(26) Almohammed, S.; Fedele, S.; Rodriguez, B. J.; Rice, J. H. Aligned Diphenylalanine Nanotube – Silver Nanoparticle Templates for High - Sensitivity Surface - Enhanced Raman Scattering. *Journal of Raman Spectoscopy*. **2017**, *48,* 1799–1807.
(27) Almohammed, S.; Oladapo, S. O.; Ryan, K.; Kholkin, A. L.; Rice, J. H.; Rodriguez, B. J. Wettability Gradient-Induced Alignment of Peptide Nanotubes as Templates for Biosensing Applications. *RSC Adv.* **2016**, *6* (48), 41809–41815.
(28) Almohammed, S.; Zhang, F.; Rodriguez, B. J.; Rice, J. H. Photo-Induced Surface-Enhanced Raman Spectroscopy from a Diphenylalanine Peptide Nanotube-Metal Nanoparticle Template. *Scientific Reports* **2018**, *8* (1), 3880.
(29) Li, P.; Chen, X.; Yang, W. Graphene-Induced Self-Assembly of Peptides into Macroscopic Scale Organized Nanowire Arrays for Electrochemical NADH Sensing. *Langmuir* **2013**, *29* (27), 8629–8635.
(30) Kagan, M. R.; McCreery, R. L. Reduction of Fluorescence Interference in Raman Spectroscopy via Analyte Adsorption on Graphitic Carbon. *Analytical Chemistry* **1994**, *66* (23), 4159–4165.
(31) Yang, H.; Hu, H.; Ni, Z.; Poh, C. K.; Cong, C.; Lin, J.; Yu, T. Comparison of Surface-Enhanced Raman Scattering on Graphene Oxide, Reduced Graphene Oxide and Graphene Surfaces. *Carbon* **2013**, *62*, 422–429.
(32) Sil, S.; Kuhar, N.; Acharya, S.; Umapathy, S. Is Chemically Synthesized Graphene 'Really' a Unique Substrate for SERS and Fluorescence Quenching? *Scientific Reports* **2013**, *3* (1), 3336.
(33) Gan, Z.; Wu, X.; Zhu, X.; Shen, J. Light-Induced Ferroelectricity in Bioinspired Self-Assembled Diphenylalanine Nanotubes/Microtubes. *Angewandte Chemie - International Edition* **2013**, *52* (7), 2055–2059.
(34) Kholkin, A.; Amdursky, N.; Bdikin, I.; Gazit, E.; Rosenman, G. Strong Piezoelectricity in Bioinspired Peptide Nanotubes. *ACS Nano* **2010**, *4* (2), 610–614.
(35) Sriram, S.; Bhaskaran, M.; Chen, S.; Jayawardhana, S.; Stoddart, P. R.; Liu, Z.; Medhekar, N. V; Kalantar-zadeh, K.; Mitchell, A. Influence of Electric Field on SERS : Frequency Effects , Intensity Changes , and Susceptible Bonds. *J. Am. Chem. Soc.* **2012**, 4646–4653.
(36) Sriram, S. Electric Field Induced Surface-Enhanced Raman Spectroscopy for Multianalyte Detection. *Physical Chemistry Chemical Physics* **2015**, *17* (11), 7095–7099.
(37) Zhao, X.; Chen, M. DFT Study on the Influence of Electric Field on Surface-Enhanced Raman Scattering from Pyridine-Metal Complex. *Journal of Raman Spectroscopy* **2014**, *45* (1), 62–67.
(38) Balaguera-Gelves, M. Del R.; Perales-Perez, O. J.; Singh, S. P.; Jimenez, J. A.; Aparicio-Bolauos, J. A.; Hernandez-Rivera, S. P. Improved Low-Temperature Aqueous Synthesis of ZnO Nanorods and Their Use in SERS Detection of 4-ABT and RDX. *Materials Sciences and Applications* **2013**, *04* (01), 29–38.
(39) Osawa, M.; Matsuda, N.; Yoshii, K.; Uchida, I. Charge Transfer Resonance Raman Process in Surface-Enhanced Raman Scattering from p-Aminothiophenol Adsorbed on

Silver: Herzberg-Teller Contribution. *Journal of Physical Chemistry* **1994**, *98* (48), 12702–12707.
(40) Kim, K.; Lee, S. H.; Kim, K. L.; Shin, K. S. Visible Light Response of Silver 4-Aminobenzenethiolate and Silver 4-Dimethylaminobenzenethiolate Probed by Raman Scattering Spectroscopy. *Journal of Raman Spectroscopy* **2013**, *44* (4), 518–524.
(41) Sooraj, K. P.; Ranjan, M.; Rao, R.; Mukherjee, S. Applied Surface Science SERS Based Detection of Glucose with Lower Concentration than Blood Glucose Level Using Plasmonic Nanoparticle Arrays. *Applied Surface Science* **2018**, *447*, 576–581.
(42) Luo, C.; Chen, Y.; Zhang, X.; Jiang, C.; Liu, Z.; Dong, S.; Zhang, X.; Xiao, X.; Yang, S.; Wang, F. Volume-Enhanced Raman Scattering Detection of Viruses. *Small* **2019**, *1805516*, 1805516.
(43) Madzharova, F.; Heiner, Z.; Guhlke, M.; Kneipp, J. Surface-Enhanced Hyper-Raman Spectra of Adenine, Guanine, Cytosine, Thymine, and Uracil. *Journal of Physical Chemistry C* **2016**, *120* (28), 15415–15423.
(44) Ten, G. N.; Burova, T. G.; Baranov, V. I. Calculation and Analysis of Vibrational Spectra of Adenine – Thymine , Guanine – Cytosine , and Adenine – Uracil Complementary Pairs in the Condensed State. *Journal of Applied Spectroscopy* **2009**, *76* (1), 84–92.
(45) Fazio, B.; Andrea, C. D.; Foti, A.; Messina, E.; Irrera, A.; Donato, M. G.; Villari, V.; Micali, N.; Maragò, O. M.; Gucciardi, P. G. SERS Detection of Biomolecules at Physiological PH via Aggregation of Gold Nanorods Mediated by Optical Forces and Plasmonic Heating. *Scientific Reports* **2016**, 7, 1–13.
(46) Boushell, V.; Pang, S.; He, L. Aptamer-Based SERS Detection of Lysozyme on a Food-Handling Surface. *Journal of Food Science* **2017**, *82* (1), 225–231.
(47) Shamsipur, M.; Farzin, L.; Tabrizi, M. A. Ultrasensitive Aptamer-Based on-off Assay for Lysozyme Using a Glassy Carbon Electrode Modified with Gold Nanoparticles and Electrochemically Reduced Graphene Oxide. *Microchimica Acta* **2016**, *183* (10), 2733–2743.
(48) Li, L. D.; Chen, Z. B.; Zhao, H. T.; Guo, L.; Mu, X. An Aptamer-Based Biosensor for the Detection of Lysozyme with Gold Nanoparticles Amplification. *Sensors and Actuators, B: Chemical* **2010**, *149* (1), 110–115.
(49) Vasilescu, A.; Gáspár, S.; Gheorghiu, M.; David, S.; Dinca, V.; Peteu, S.; Wang, Q.; Li, M.; Boukherroub, R.; Szunerits, S. Surface Plasmon Resonance Based Sensing of Lysozyme in Serum on Micrococcus Lysodeikticus-Modified Graphene Oxide Surfaces. *Biosensors and Bioelectronics* **2017**, *89*, 525–531.
(50) Rezaei, B.; Jamei, H. R.; Ensafi, A. A. Lysozyme Aptasensor Based on a Glassy Carbon Electrode Modified with a Nanocomposite Consisting of Multi-Walled Carbon Nanotubes, Poly(Diallyl Dimethyl Ammonium Chloride) and Carbon Quantum Dots. *Microchimica Acta* **2018**, *185*, 180.
(51) Muniz-Miranda, M. SERS Monitoring of the Catalytic Reduction of 4-Nitrophenol on Ag-Doped Titania Nanoparticles. *Applied Catalysis B: Environmental* **2014**, *146*, 147–150.

Supporting Information

Electric Field-Induced Chemical Surface-Enhanced Raman Spectroscopy from Aligned Peptide Nanotube–Graphene Oxide Templates for Universal Trace Detection of Biomolecules

Sawsan Almohammed [a, b], Fengyuan Zhang [a, b], Brian J. Rodriguez * [a, b], and James H. Rice * [a]

[a]School of Physics, University College Dublin, Belfield, Dublin 4, Ireland
[b]Conway Institute of Biomolecular and Biomedical Research, University College Dublin, Belfield, Dublin 4, Ireland

*e-mail correspondence to brian.rodriguez@ucd.ie and james.rice@ucd.ie

Device fabrication, gold sputtering through 3D printed mask

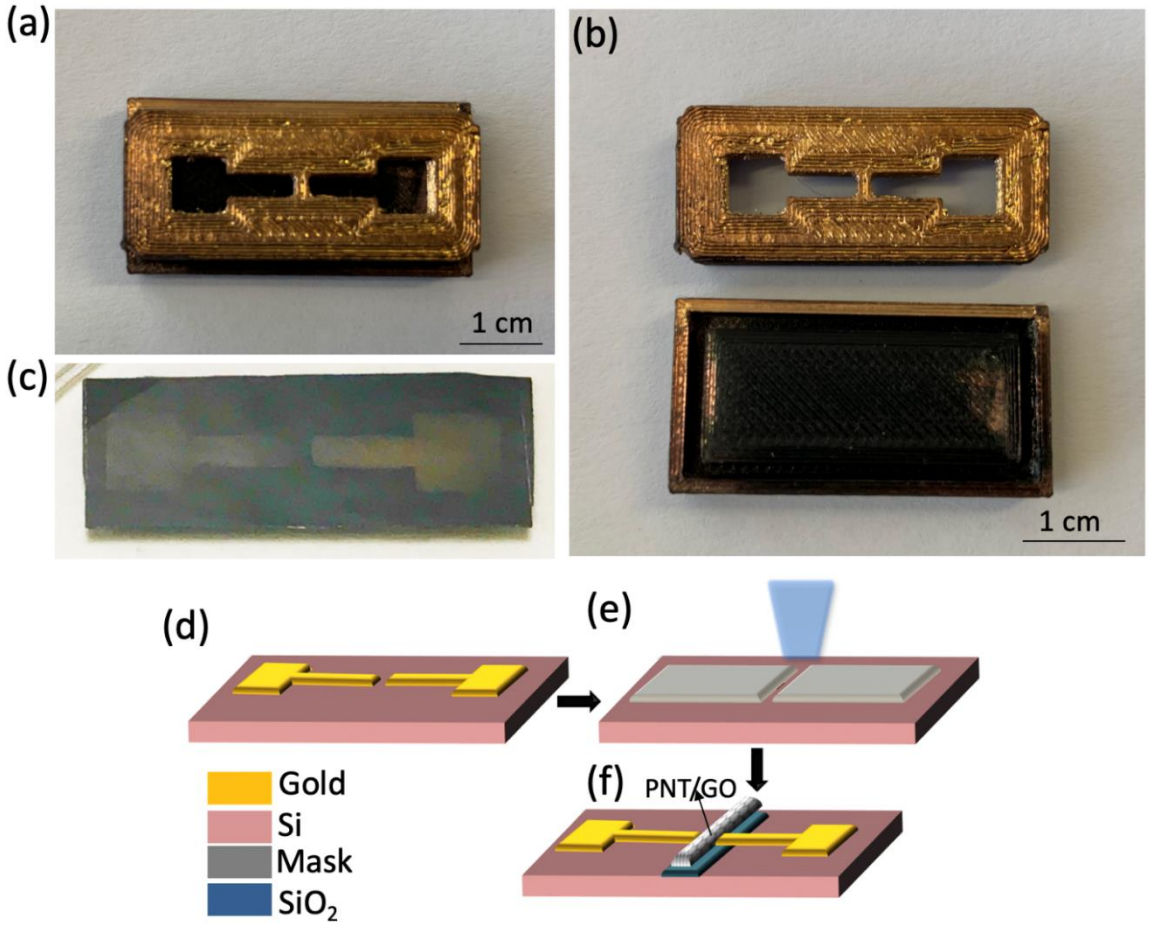

Figure S1. (a) 3D printed mask, with ~ 0.1 mm opening, for gold electrode deposition. (b) The two layers of the mask where the Si substrate was placed. (c) Si substrate after gold deposition. (d) Schematic showing the substrate with gold electrodes. (e) UV/ozone was used to form SiO_2 through a physical mask comprising two pieces of Si, with 1 mm opening. (f) Deposition of FF-PNT/GO in the hydrophilic region between the gold electrodes.

Substrate features

To verify the formation of FF-PNT/GO nanocomposites prepared as outlined in Fig. S1, we visualized the structure of the composite and the starting materials using a scanning electron microscope (SEM) (Figs. S2 and S3) and atomic force microscopy (AFM) (Fig. S4).

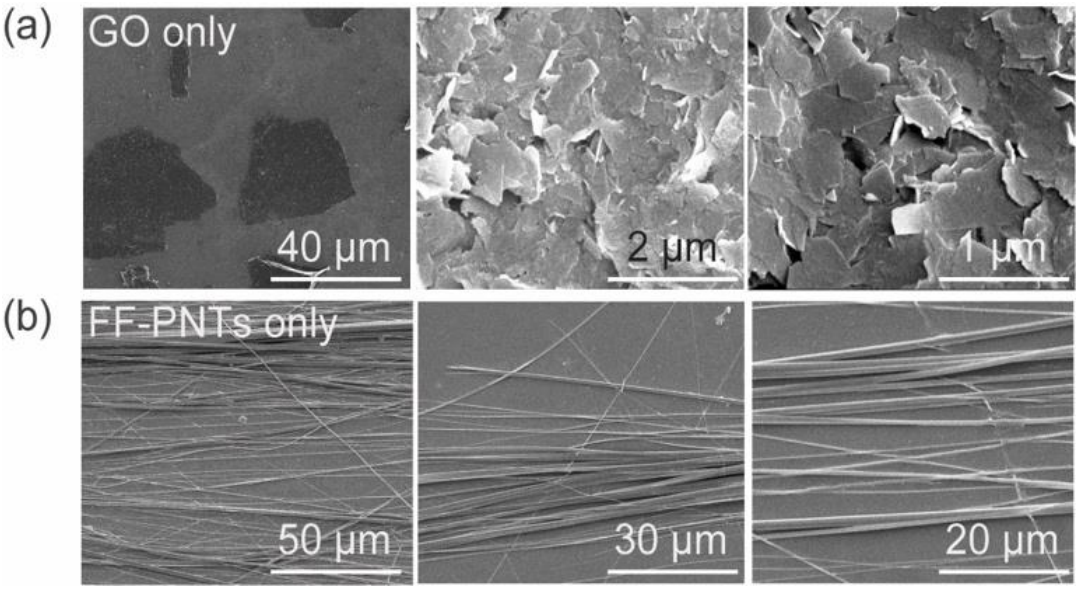

Figure S2. SEM images of (a) GO and (b) FF-PNTs separately. GO only in the absence of FF-PNTs appears as flakes in SEM images. In contrast, FF-PNTs only (in the absence of GO) show tube structures with diameters of 3.8 ± 1.4 µm from n = 30 FF-PNTs.

The disappearance of the GO flakes after the addition of FF-PNT and the smaller size of the tubes is consistent with FF-PNT/GO assembly (at GO concentration: 0.5, 1 or 2 mg/ml).[9–13,27–29] The resulting nanotubes are determined to possess diameters of ~ 1 µm by SEM (Fig. S3).

It is widely accepted that FF-PNTs form through rolling of peptide sheets to enclose hydrophilic channels and to stack the hydrophobic phenyl rings.[1–4,27–29] The hydrophilic nature of GO sheets makes it likely that they would incorporate in these hollow channels during the self-assembly process.[1–4,27–29] Although it is difficult to discern from SEM (Fig. S3), it is expected that the hydrophilic nature of the inner channels of the FF-PNTs could be the primary region of interaction with the GO. Increasing the GO concentration added to the FF-PNTs may influence the final structure of the tubes, potentially producing a layered composite structure of GO interleaved between a multi-walled FF-PNTs structures, as previously reported for amyloid-graphene nanocomposites.[5–8]

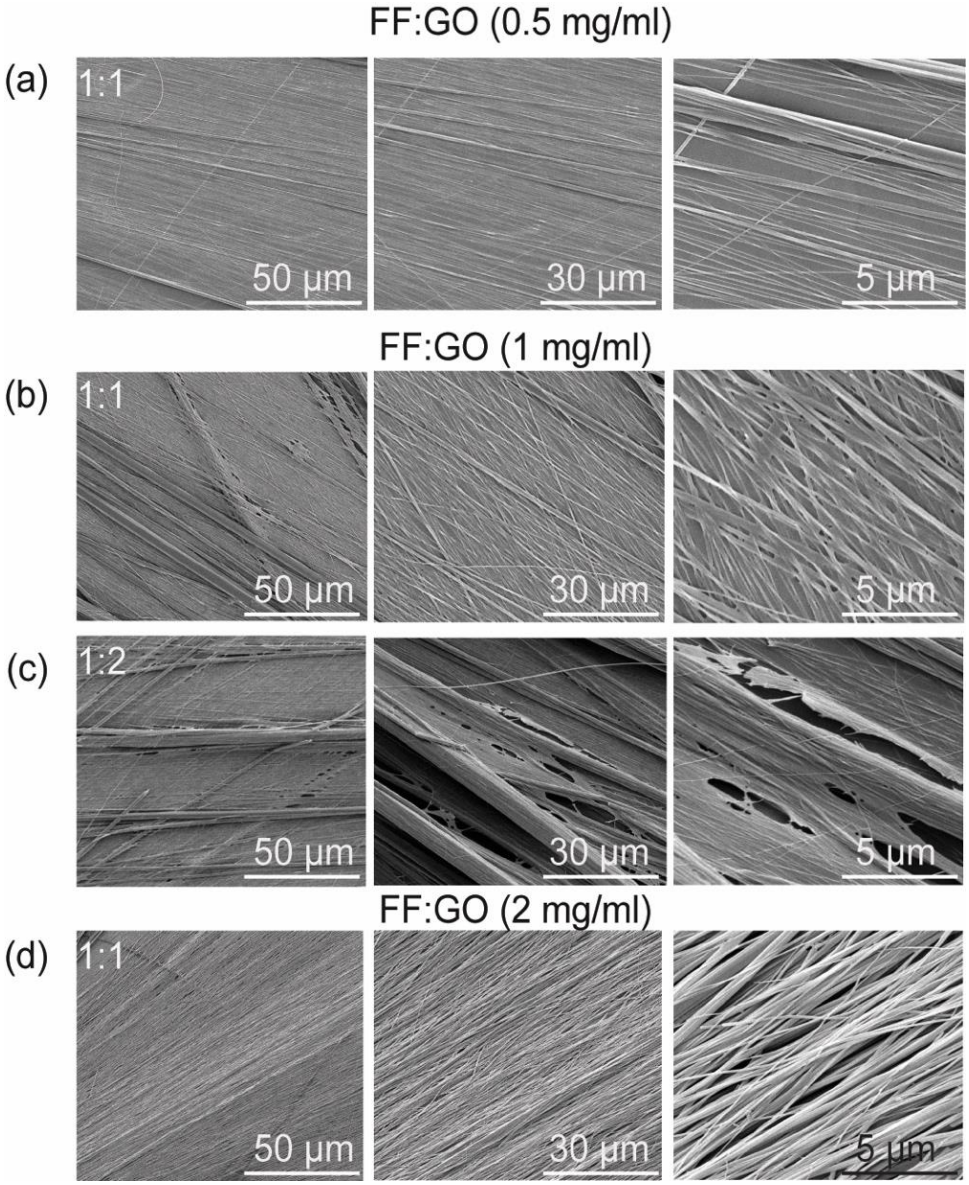

Figure S3. SEM images of FF-PNT/GO nanocomposites at different GO concentrations: (a) 0.5 mg/ml GO, (b) and (c) at 1 mg/ml GO at 1:1 (FF: GO) and 1:2 (FF: GO) ratios, respectively, and (d) at 2 mg/ml GO.

The AFM image in Fig. S4b was recorded from the same nanotube cluster shown in Fig. S4a. The coverage area of the nanotubes is 68.5 % (in the presence of GO) and 31 % (in the absence of GO (Fig. S4e)), as calculated from the 30 µm scans. The PFM amplitude image in Fig. S4c shows strong lateral piezoresponse on the nanotubes (in yellow). A uniform polarization direction (purple) is shown in the PFM phase image in Fig. S4d. This suggests that the nanotube cluster shown in Fig. S4a has a uniform polarization direction. The surface roughness of the FF-PNT/GO template, as determined from AFM, is 108.1 nm.

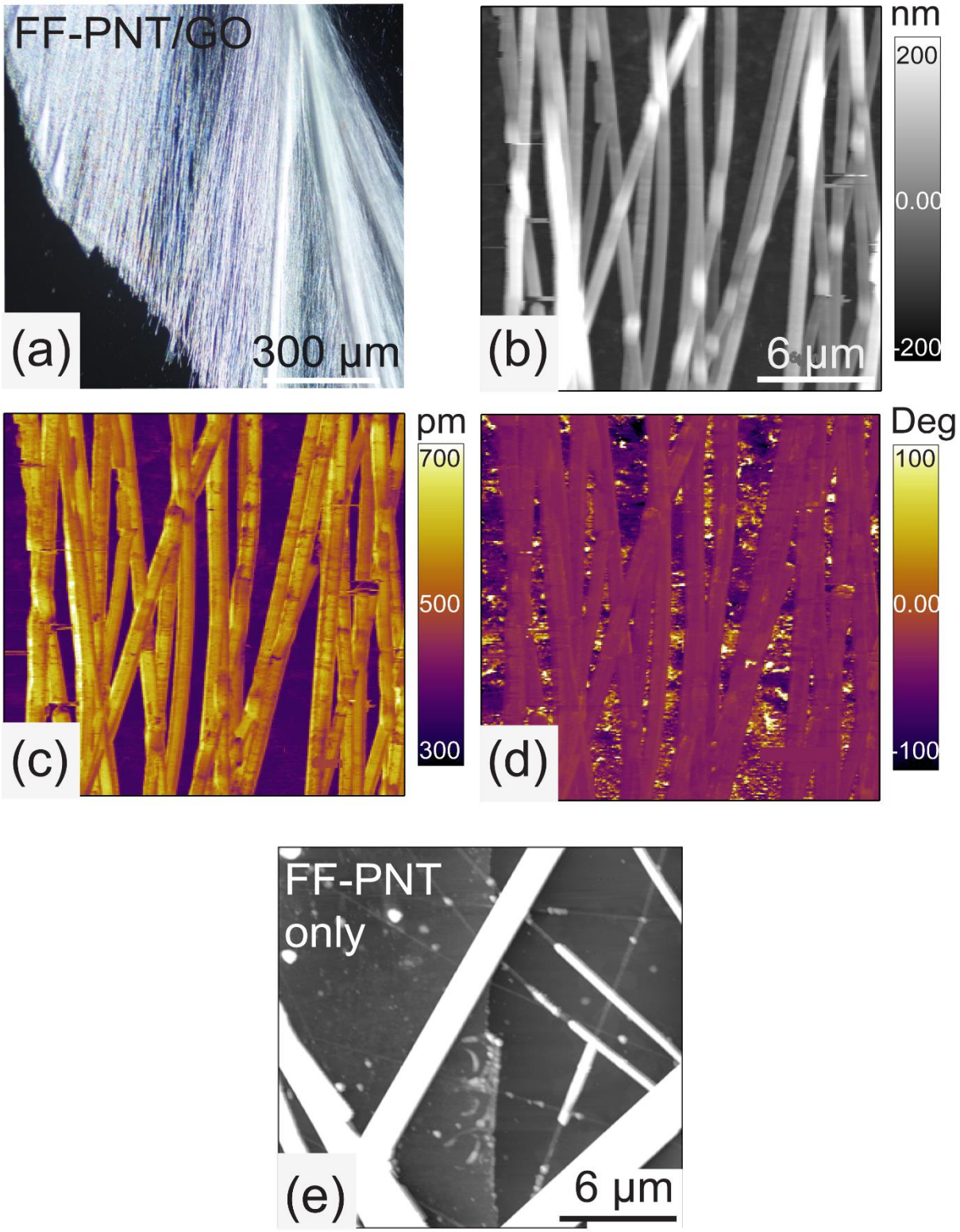

Figure S4. (a) Optical image FF-PNT/GO (1:1), with 10x objective. (b) Atomic force microscopy (AFM) height and lateral piezoresponse force microscopy (PFM) (c) amplitude and (d) phase images recorded with an AFM (MFP-3D, Asylum Research) using a lock-in amplifier (HF2LI, Zurich Instruments) and a CSC37-Pt probe, cantilever B (MikroMasch). In-plane PFM images were recorded with a 10 kHz ac voltage of 30 V. (e) AFM image of FF-PNTs only.

Conductivity of the substrate

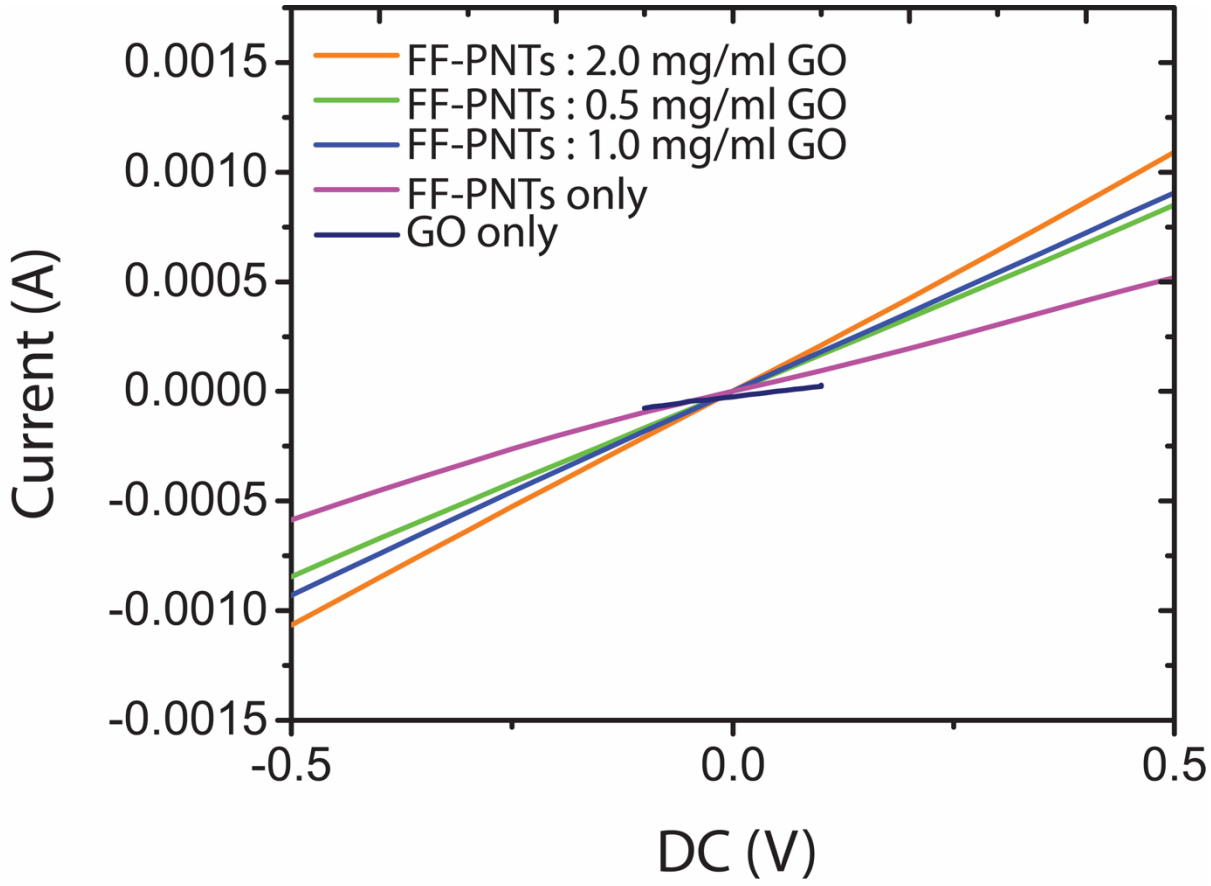

Figure S5. Current-voltage (IV) measurements of FF-PNT (2 mg/ml) / GO samples at different GO concentrations: 2 mg/ml (orange), 0.5 mg/ml (green), 1 mg/ml (blue), FF-PNTs only (purple), and GO only (dark blue). The plot was recorded using a Keithley 2400 SourceMeter. The samples were connected to the source meter directly to the electrodes via alligator clips.

Current-voltage (IV) measurements (Fig. S5) of the aligned FF-PNT/GO revealed Ohmic behavior, with resistances of 593.23 ± 0.58 Ω (FF-PNT; 0.5 mg/ml GO), 547.12 ± 0.78 Ω (FF-PNT; 1 mg/ml GO), and 466.03 ± 0.68 Ω (FF-PNT; 2 mg/ml GO). The resistance for GO alone was 1396.02 ± 1.92 Ω and for FF-PNTs alone the resistance was 930.02 ± 1.03 Ω. These values are in agreement with reports that the resistance of FF-PNTs is lowered with the incorporation of semiconductors or metal nanoparticles.[1–4,9] These results demonstrate the possibility of using FF-PNT/GO nanocomposites in electronic devices and as a platform to explore the influence of applied electric field on GO-based SERS substrates.

FTIR and absorption studies of the substrate

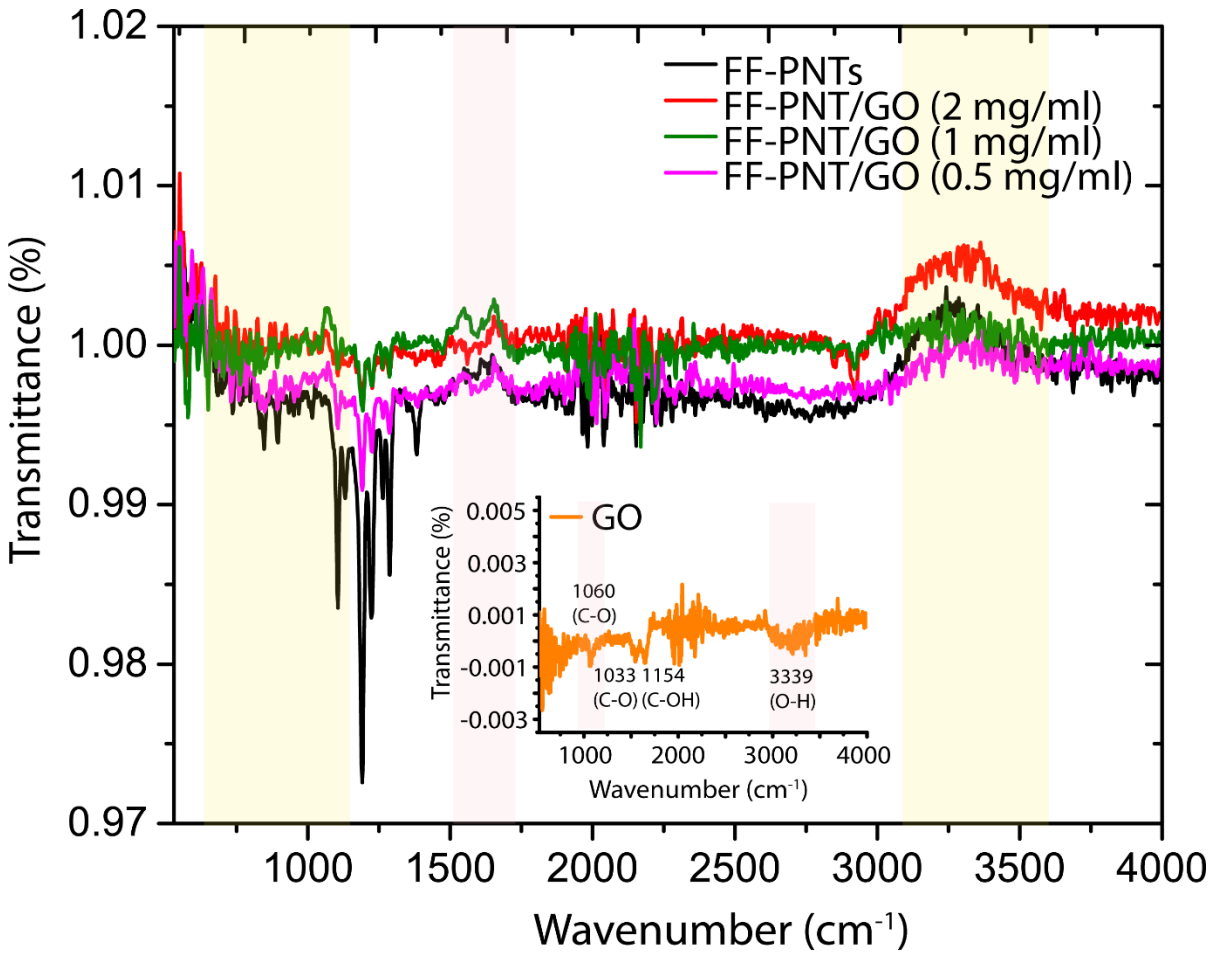

Figure S6. ATR-FTIR spectrum of FF-PNTs recorded in aqueous solution with GO at different concentrations (red, 2mg/ml; green, 1 mg/ml; and pink, 0.5 mg/ml) and without GO (black), showing that the presence of GO does not change the chemical structure or formation of FF-PNTs. The broad nature of the amide I band at 3250 cm^{-1} corresponds to a β-sheet structure. The inset shows FTIR spectrum of GO only.

FTIR measurements performed on FF-PNT solutions with and without GO (Fig. S6) demonstrate that the spectral features remain unchanged following the addition of GO. The spectral features are similar to those reported for FF-PNTs. FTIR modes at 1730 and 3400 cm^{-1} and modes from 1380 – 1460 cm^{-1} are attributed to the stretching of C=O bonds, O–H bonds, and the stretching modes of the C-OH bonds of carbonyl and carboxylic acid, respectively.[5–7] FTIR spectra of GO only showed a broad band at 3338 cm^{-1}, which belongs to a strong stretching mode of OH, another peak at 1635 cm^{-1} due to C=C stretching, and peaks at 1716, 1154, and 1033 cm^{-1}, which correspond to the stretching modes of C=O, C–OH, and C–O, respectively.[10] Theoretical and experimental studies have revealed that the aromatic rings of amino acids prefer to orient parallel to the GO basal plane, which bears the signature of weak π–π stacking. The polarizability of amino acids may play a role in the binding strength with GO, which has implications in biosensor design using these combined materials.[1–4,27–29] It has been demonstrated that FF-PNTs bind to GO through electrostatic interactions.[1–4,27–29]

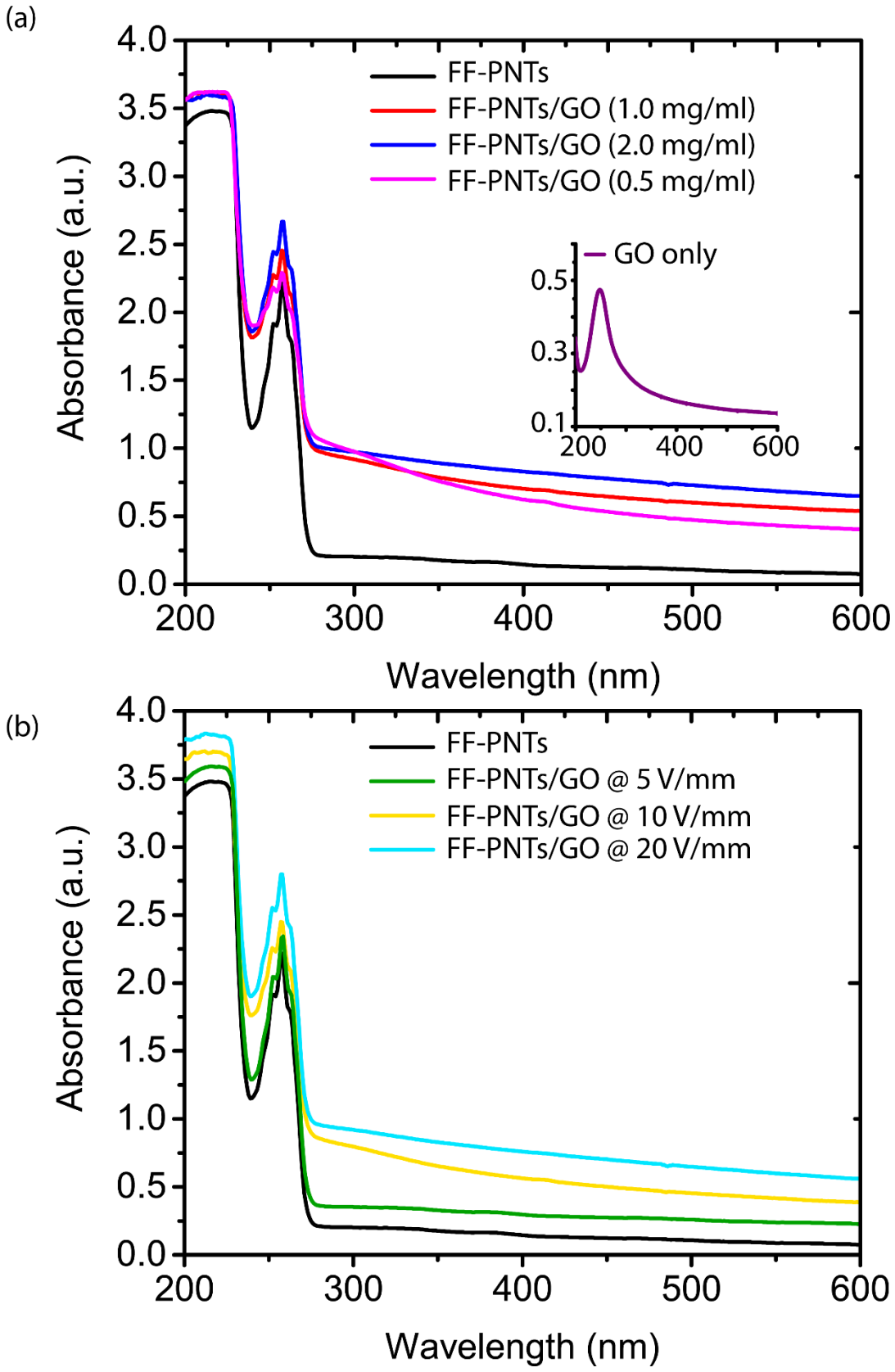

Figure S7. Optical absorption measurements of FF-PNT/GO composites with (a) no electric at different ratios and (b) with applied electric fields on a cover slip. The inset in a shows UV-vis absorption spectra of aqueous GO solution in a quartz cuvette with a sharp absorption peak at ~ 233 nm.

The optical absorption spectra of FF-PNT and GO solutions have been recorded separately (Fig. S7). The absorption spectrum for GO alone (Fig. S7a inset) shows an absorption peak at ~ 233 nm, which arises from $\pi-\pi^*$ transitions of the aromatic C=C bond and a shoulder at ~ 300 nm corresponding to $n-\pi^*$ for the C=O bond transition.[9] In contrast, the absorption spectrum for FF-PNTs alone is transparent over the visible range with absorption peaks at ~ 222 and ~ 260 nm due to $\pi-\pi^*$ electronic transitions of the phenyl group, in agreement with previous reports.[5–7] For FF-PNT/GO, there were no observable changes in the absorption spectra compared to FF-PNTs only; a slight increase of ~ 20 % in the absorption peak intensities was observed with the addition of GO. With applied electric field, however, a significant increase of ~ 70 % in intensity was observed.

These results suggest that higher concentration of GO could provide more $\pi-\pi$ conjugation and hydrogen bonding.[11] Previous studies have shown that since the self-assembly of FF monomers involves both hydrogen bonding interactions and $\pi-\pi$ stacking of aromatic residues, the presence of higher concentrations of GO could potentially affect the self-assembly of FF and result in the formation of smaller diameter tubes.[11]

SERS signal increase with an applied electric field

Concentrations as low as 0.1 µM were deposited above the dried aligned FF-PNT/GO composite located between the gold electrodes for Raman measurements to be performed. Significant enhancement in SERS intensity was seen at applied electric fields of 5 – 25 V/mm, whereas a reduction in signal intensity was observed for applied fields between 30 – 50 V/mm.

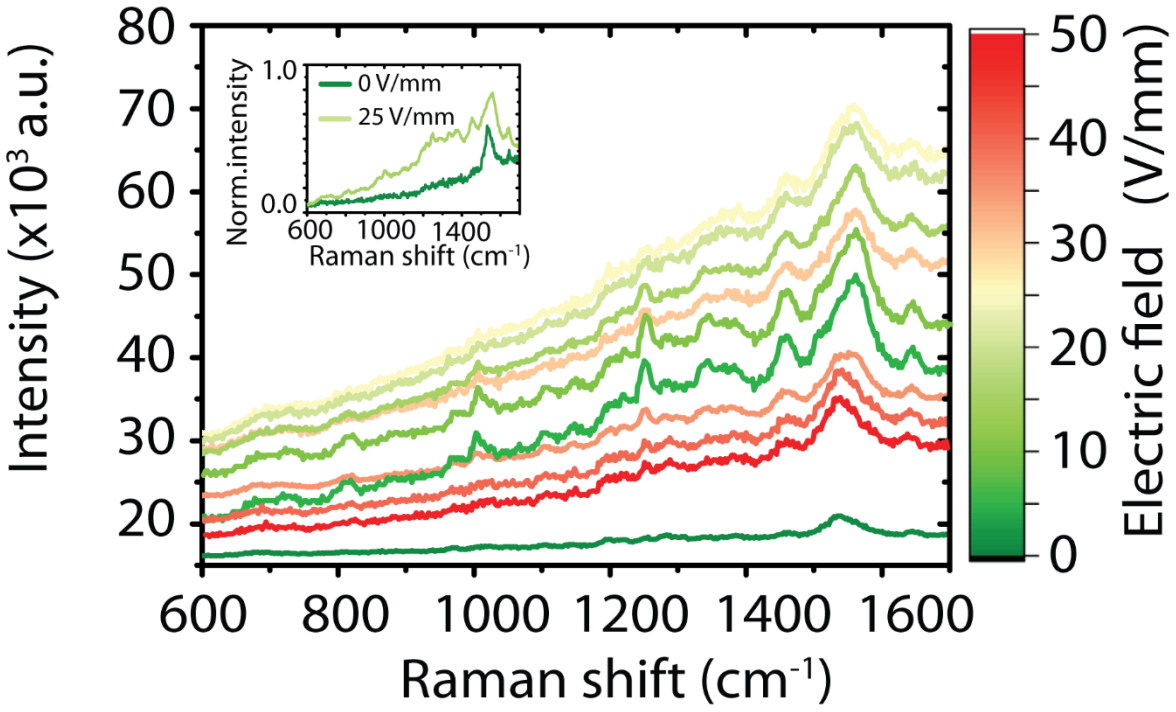

Figure S8. SERS from the probe molecule meso-tetra (N-methyl-4-pyridyl) porphine tetrachloride (TMPyP at ~ 0.1 µM) on the FF-PNT/GO substrate at a 100 nanomolar concentration.

Raman bands arising from TMPyP were clearly visible and distinguishable, including bands at 1249 cm^{-1} (C-pyrrole bending), 1451 cm^{-1} (C–C stretching), 1573 cm^{-1} (C–C stretching) and 1639 cm^{-1} (pyrrole bending).[5–7] TMPyP was also investigated at a lower concentration (~ 10^{-13} M) (Fig. S8), and significant enhancement in SERS intensity was seen at electric fields applied from 5 – 25 V/mm (~ 7-fold increase), following with a reduction of signal intensity with electric fields between 30 – 50 V/mm.

Studies of additional substrate designs

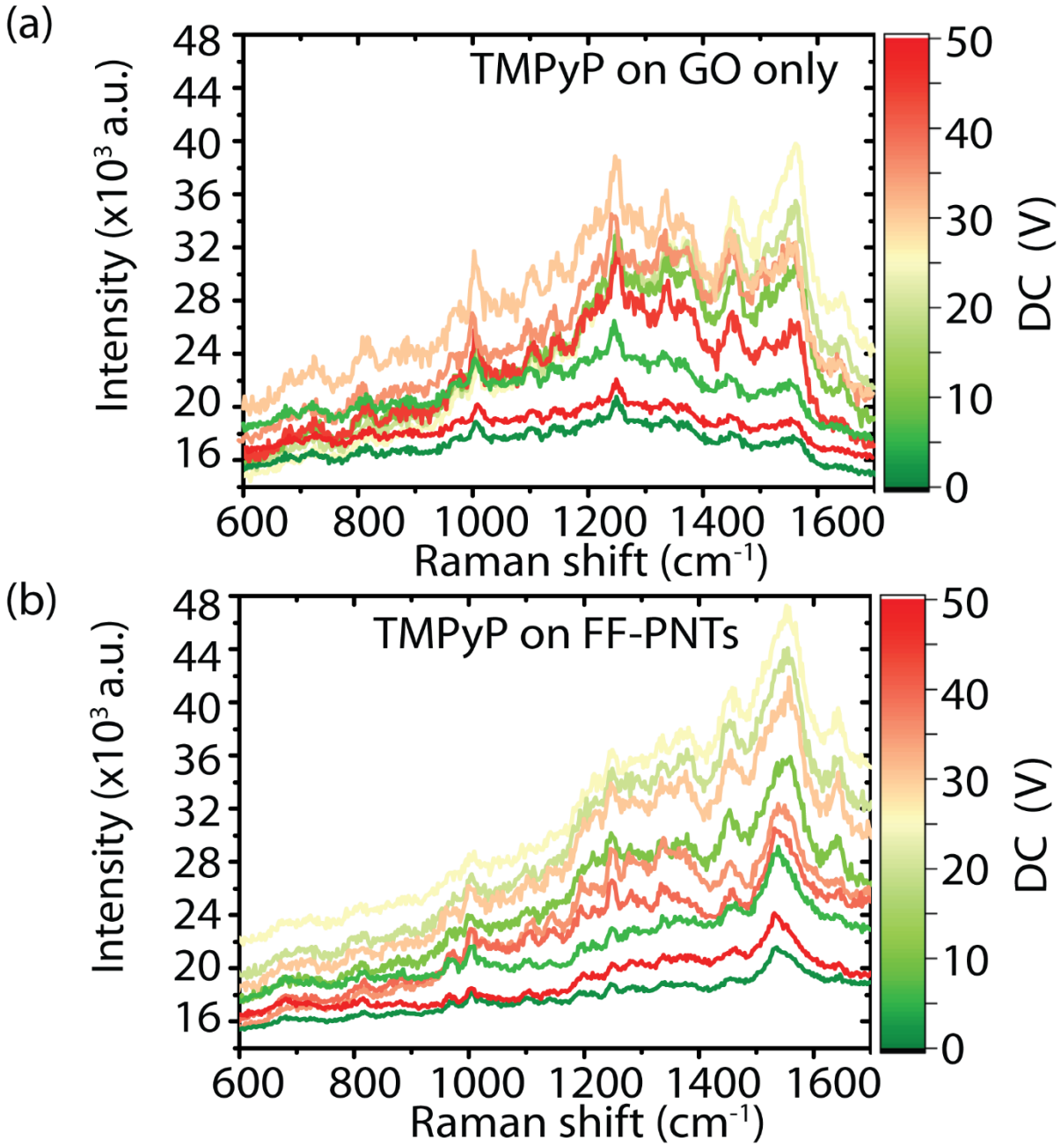

Figure S9. SERS of TMPyP at different electric fields from 0 – 50 V/mm on (a) GO only and (b) FF-PNT only.

Raman spectra for TMPyP on GO only (in the absence of FF-PNT) and for TMPyP on FF-PNTs only (in the absence of GO) with and without an applied electric field are shown in Fig. S9.

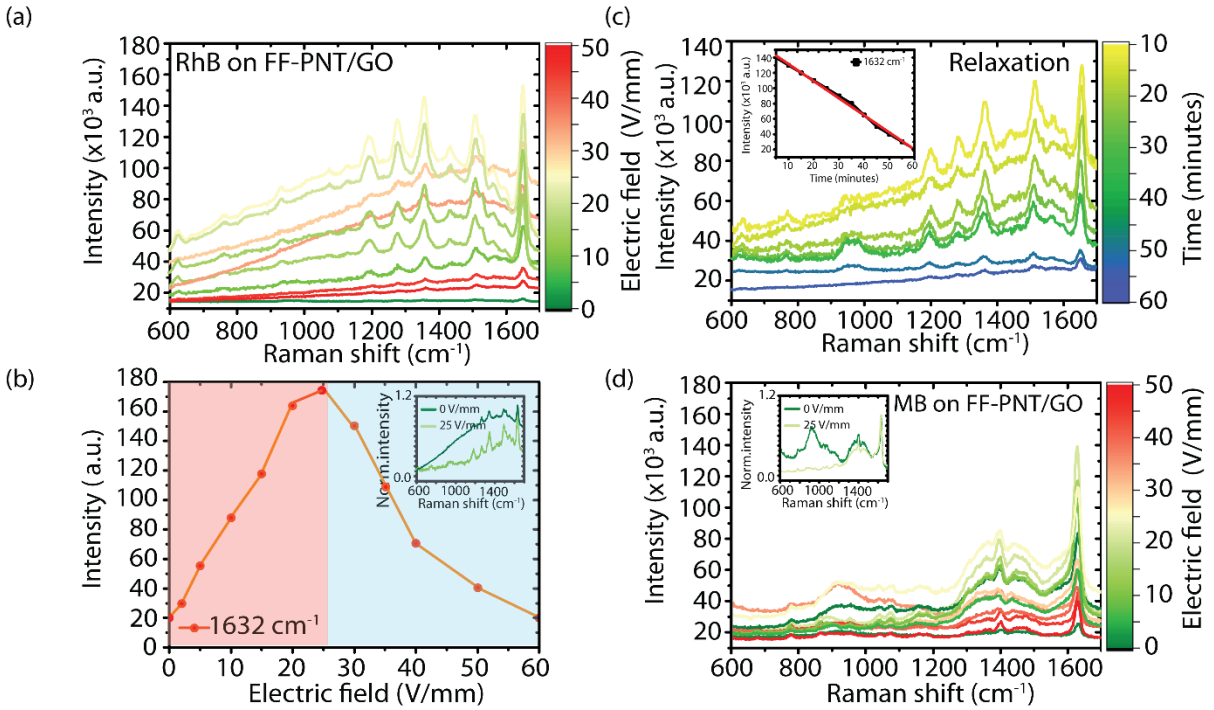

Figure S10. SERS spectra from (a-c) rhodamine B (RhB) and (d) methylene blue (MB) probe molecules on FF-PNT/GO. (a) RhB probe molecules on FF-PNT/GO on Si at electric fields from 0 – 50 or 60 V. (b) SERS intensity versus electric field. The inset shows a comparison of normalized SERS spectra at 0 V and 25 V. (c) Relaxation of SERS after removing the electric field. The inset shows a plot of the relative intensity of RhB bands at 1632 cm^{-1} as a function of the relaxation time. (d) SERS spectra from MB on FF-PNT/GO on Si as a function of applied electric field. The inset shows a comparison of SERS spectra at 0 V and 25 V.

The prominent SERS bands of RhB and MB were clearly distinguishable, including bands at 1649 cm^{-1}, 1593 cm^{-1}, 1509 cm^{-1}, 1359 cm^{-1}, and 1280 cm^{-1} (for RhB) and bands at 1621 cm^{-1} ((C–C) ring stretching), 1391 cm^{-1} and 1433 cm^{-1} ((C–N) symmetric and asymmetric stretching), and 650 cm^{-1} ((C–N–C) skeletal deformation mode) (for MB), in agreement with literature values.[10,12] Applying an electric field from 30 – 60 V/mm resulted in a reduction in SERS intensity, as was seen for TMPyP (Fig. 1). After turning off the electric field permanently, the SERS signal of RhB and MB, like TMPyP, reduced back to its original intensity over the course of 60 minutes (Fig. S10).

Heat effect and UV irradiation study of the substrate

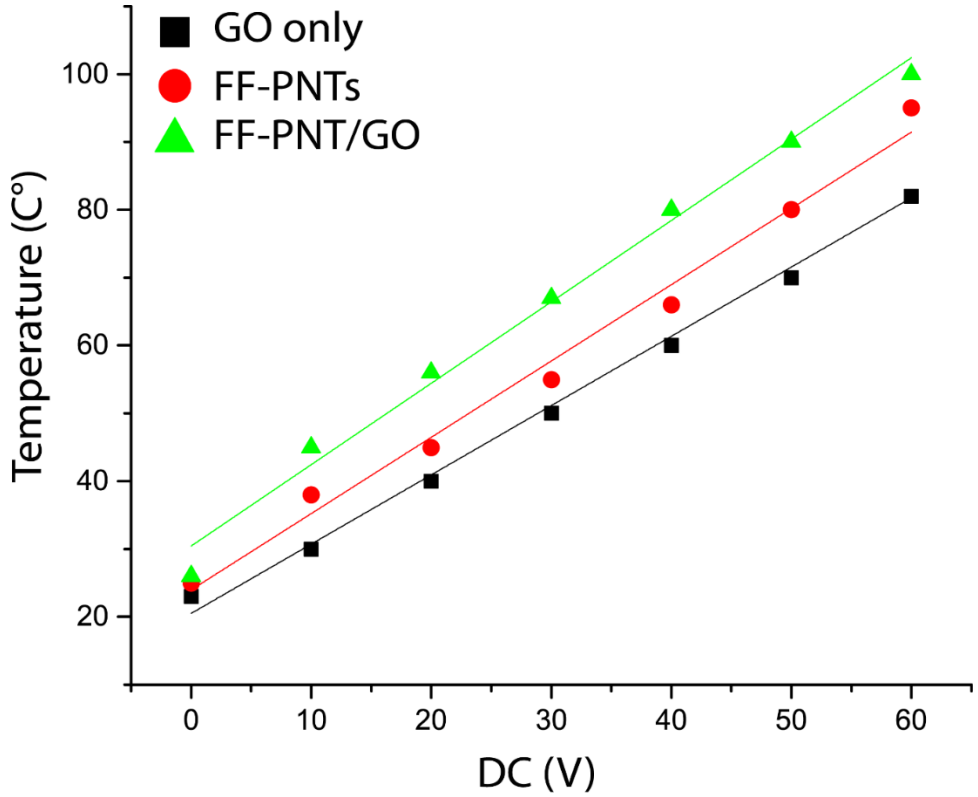

Figure S11. Plot of temperature as a function of voltage for GO only (black), FF-PNTs only (red), and FF-PNT/GO (green). The plot was fitted using a linear fit. Intercepts are 20.5 ± 1.4, 23.9 ± 1.9 and 30.4 ± 2.1 for GO only, FF-PNT only, FF-PNT/GO, respectively. The slope is 1.02 ± 0.04, 1.25 ± 0.05, and 1.20 ± 0.05 for GO only, FF-PNT only, FF-PNT/GO, respectively.

The temperature of the template was found to increase with increasing applied bias (i.e., increasing electric field), as shown in Fig. S11. It was reported that the interaction of water with FF-PNTs leads to the splitting of the conduction and valence bands that may be associated with the alignment of the water molecules' dipole moments, resulting in a larger dipole moment of the overall structure.[16–19] The presence of water molecules increases the hopping electron probabilities and, thus, may enhance conductivity. At higher temperatures, a reduction in conductivity may arise due to removal of water from the nanotubes, resulting in a reduction in conduction and consequently SERS intensity. Andrade-Filho et al.[19] has shown that the increase in temperature could possibly influence the degree of ordering of water molecules in the nanochannel of individual nanotubes. Hydrophilic interactions of water with COO^- tails are considered to be temperature-dependent and the disruption of dipole ordering occurs mainly in the inner core of water structure.[16–19] The dipolar order of water molecules located near carboxyl groups in the nanocavities cannot recover at higher temperatures (~ 60 – 100 °C) due to their high mobility, resulting in a gradual decrease of pyroelectric current and hence reduction in SERS signal.

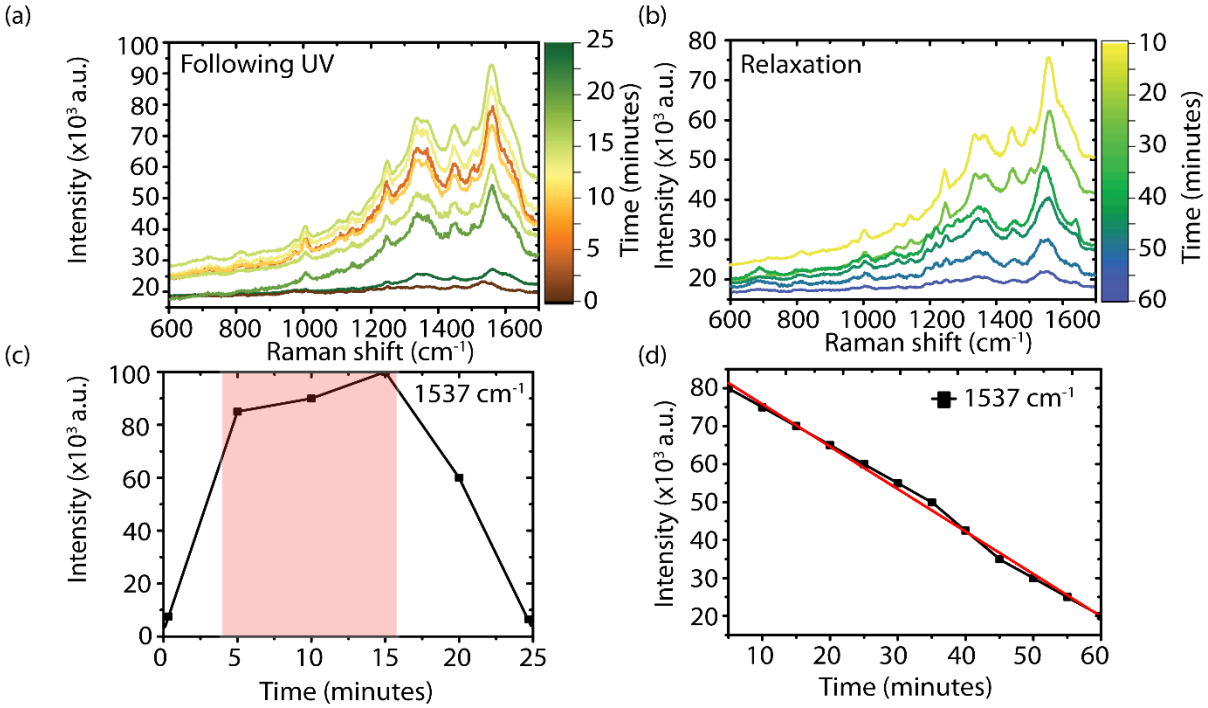

Figure S12. (a) SERS spectra from TMPyP (10^{-5} M) on FF-PNT/GO on Si following UV irradiation. (b) Relaxation over 60 minutes after turning off the UV irradiation. (c) Plot of the bands at 1537 cm^{-1} as a function of UV irradiation. (d) Plot of SERS intensity as a function of relaxation time. The red shading refers to the threshold where the maximum enhancement was seen.

The highest enhancement was recorded after ~ 15 minutes; additional UV exposure resulted in the intensity then dropping (Fig. S12). Relaxation in the SERS signal was observed after the UV irradiation source was removed and the SERS signal recovered its original intensity over ~ 60 minutes (Fig. S12). The SERS spectrum recorded after 15 minutes of UV exposure showed a small reduction in background signal compared to the SERS spectrum recorded with an applied electric field of 20 V/mm (Fig. 2), which was the field strength that gave the highest SERS signal enhancement.

Reversible control of Raman signal intensity

Returning the electric field back to lower values, e.g., to a range of 5 – 25 V/mm increased the SERS signal intensity, demonstrating reversible tuning of the SERS signal intensities with applied electric field (Fig. S13).

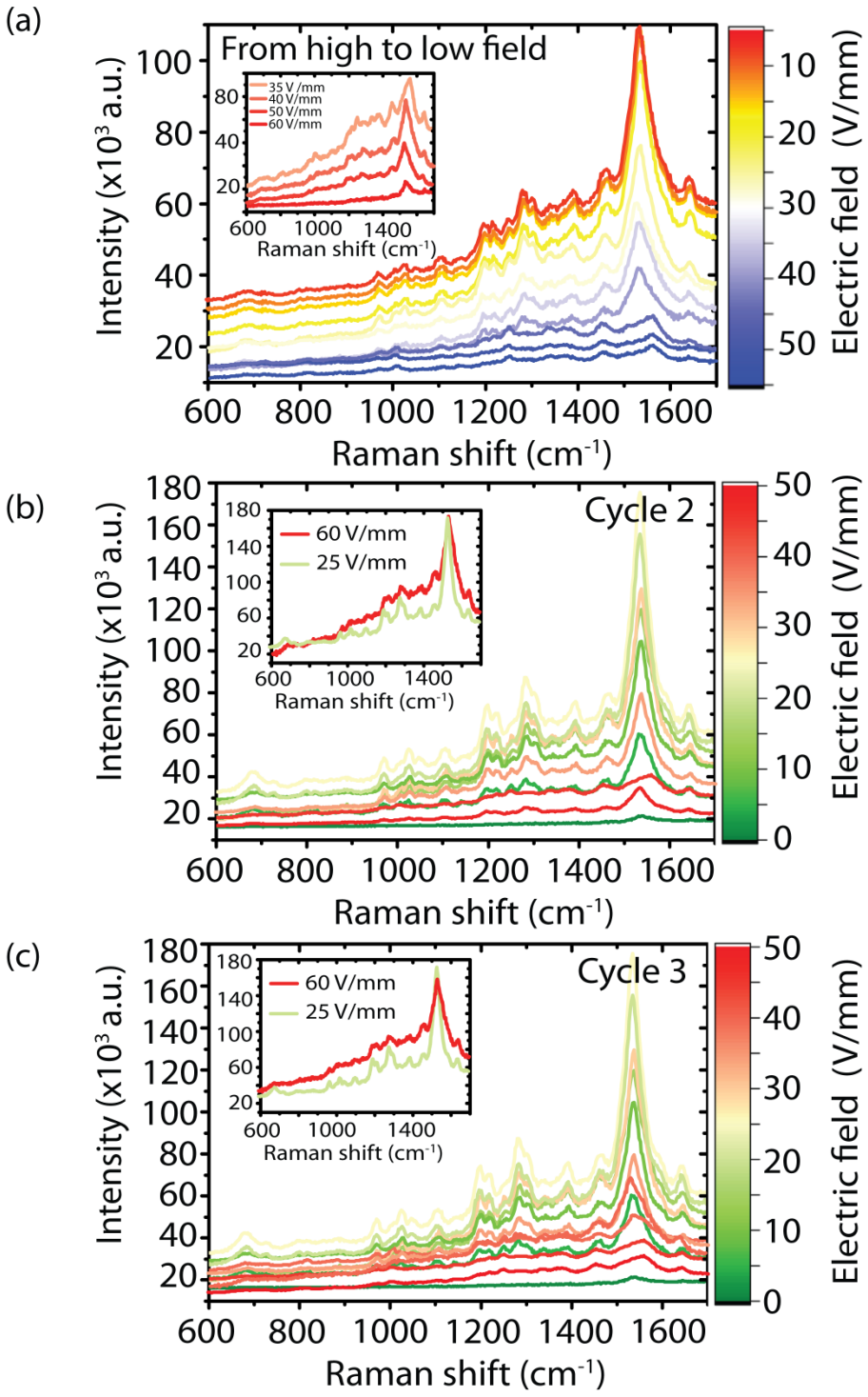

Figure S13. SERS from the probe molecule meso-tetra (N-methyl-4-pyridyl) porphine tetrachloride (TMPyP) on the FF-PNT/GO template. (a) Spectra recorded from high to low applied electric field following application of an electric field of 60 V/mm. The inset shows spectra recorded as the electric field was increased back to 60 V/mm. (b,c) Signal reproducibility (b) after cycle 1 and (c) after cycle 2. This data shows that multiple applications of electric field does not cause an observable change in the SERS spectra. SERS intensity remained stable over 3 cycles, i.e., changing the electric field from low (5 V/mm) to high values (60 V/mm) and then back to low values 3 times.

Stability and reproducibility tests were performed on the FF-PNT/GO template after two cycles of increasing the applied electric field from 0 – 60 V/mm and then reducing the electric field back from 60 – 0 V/mm (Fig. S14). The SERS signal intensity at electric fields from 5 – 35 V/mm varied < 5 % (Fig. S13). These results demonstrate that the FF-PNT/GO template is highly uniform and stable under the applied field.[13–15]

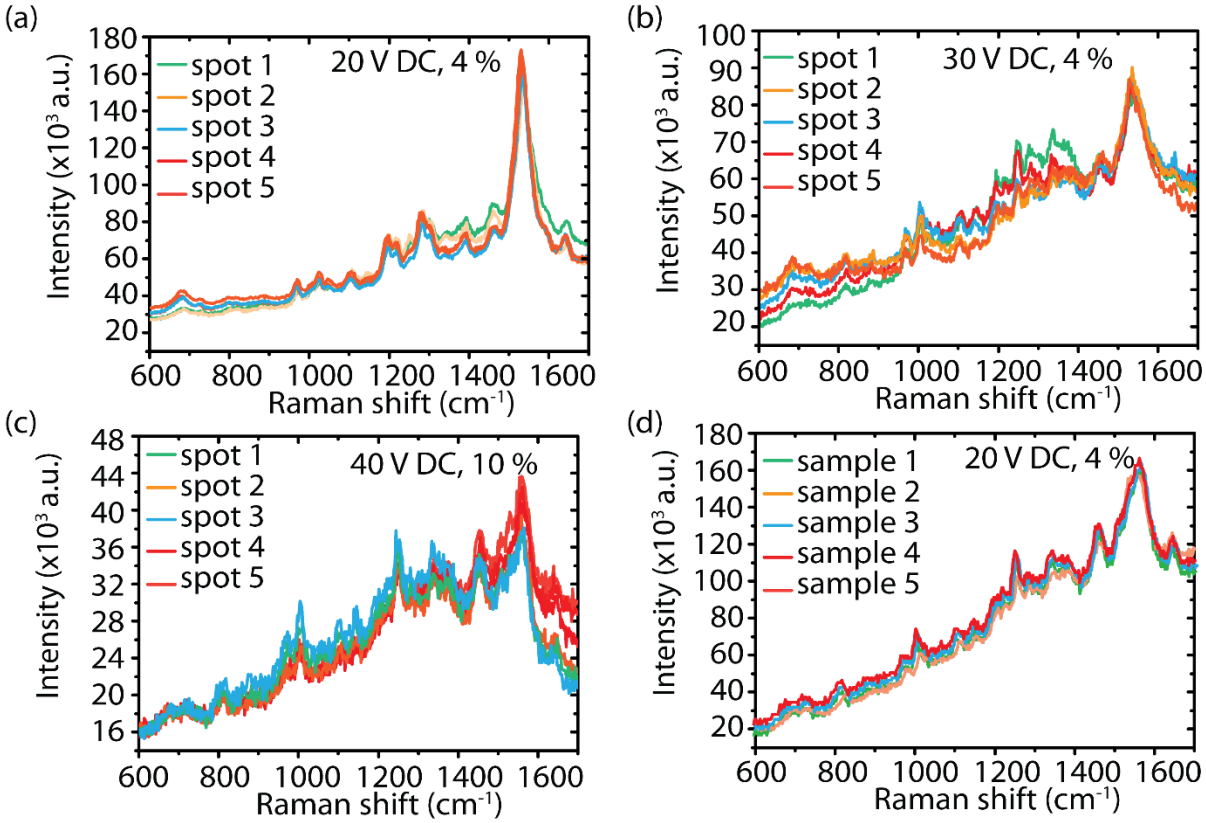

Figure S14. Uniformity and reproducibility tests of TMPyP on FF-PNT/GO templates at different electric fields at different locations or on different samples.

Charge transfer processes using the probe molecule 4-ABT

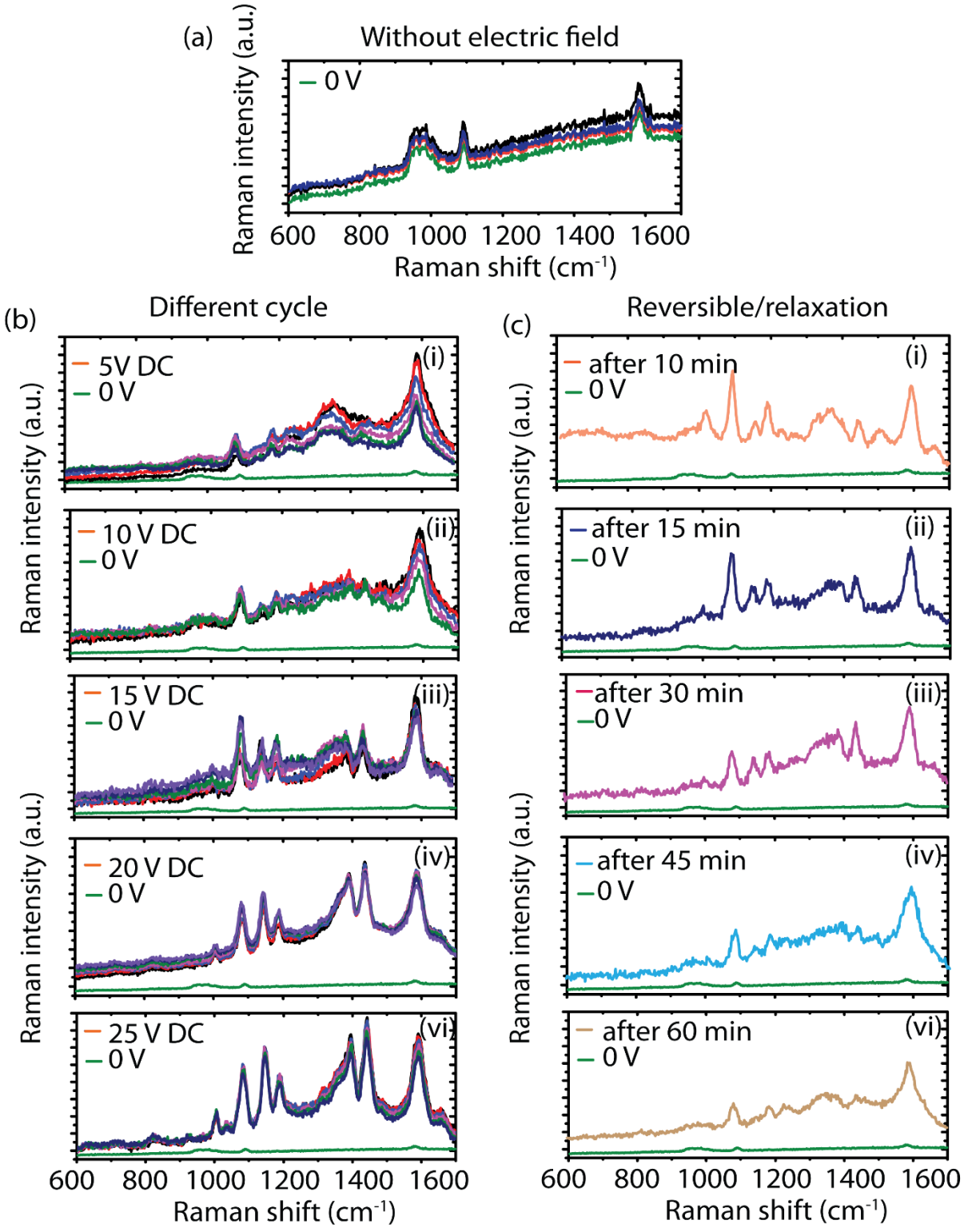

Figure S15. SERS spectra from 4-ABT probe molecules on FF-PNT/GO on Si at electric fields applied from 0 – 25 V. (a) Raman spectra recorded in the absence of an electric field, recorded from several locations on the sample. (b(i-vi)) SERS recorded for increasing electric fields. (c(i-vi)) SERS reversibility/relaxation over time.

With an applied electric field of ~ 10 V/mm, additional bands appear including five intense bands at 1590, 1432, 1390, 1144, and 1076 cm^{-1} (Fig. S15).[20,21] The band assigned to the vibrational mode with a_1 symmetry (υCS + υCC) is shifted from 1088 to 1076 cm^{-1} with an applied electric field.[20,21] A band at 1181 cm^{-1} is also observed and is assigned to an a_1 symmetry (δCH). The broad band around 1590 cm^{-1} is formed by two modes assigned to υCC. In comparison, no 4-ABT Raman bands can be seen from 4-ABT on GO only with or without an applied electric field (Fig. S16).

The effect of the applied electric field on the Raman enhancement was found to be reversible for 4-ABT as well. Under an electric field of 25 V/mm, a significant increase in Raman intensity was observed (Fig. S15). After relaxation and by applying electric field again from 5 – 25 V/mm, the appearance of intense b_2 Raman bands can again be seen, showing that the template exhibits fully reversible behavior.

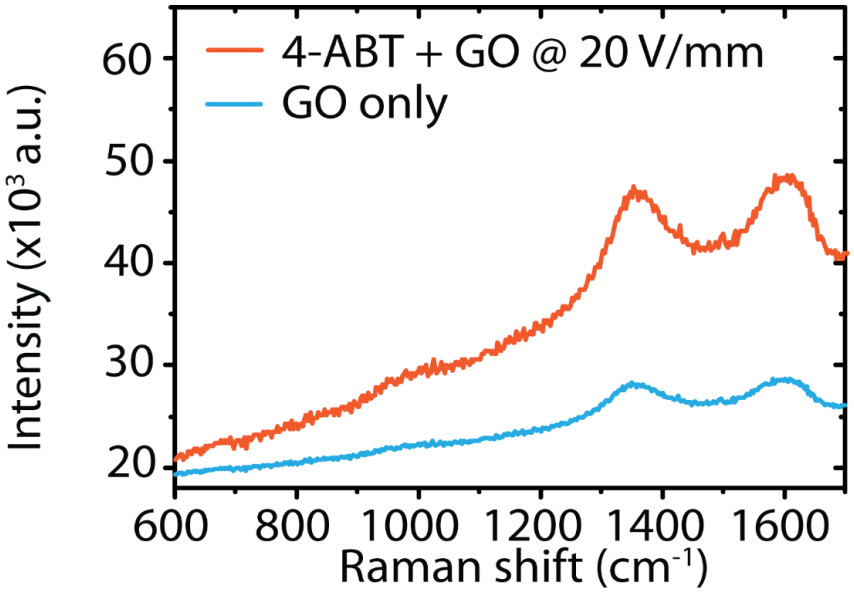

Figure S16. SERS spectra from 4-ABT on GO only on Si at an electric field of 25 V/mm, showing only the D- and G-bands of GO.

Studies of FF-PNT/GO with applied field in absence of a probe molecule

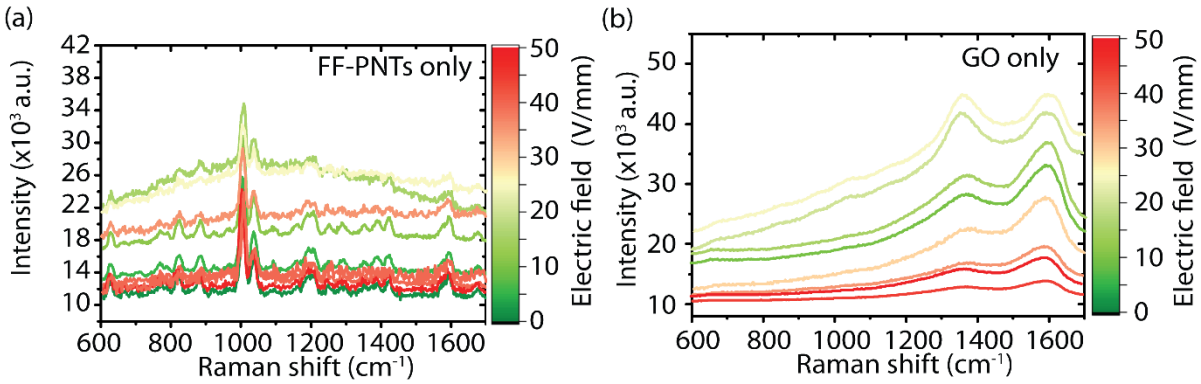

Figure S17. (a) Raman of FF-PNTs only at different electric fields from 0 – 50 V/mm. (b) Raman of GO only at different electric fields from 0 – 50 V/mm.

SERS measurements were performed on FF-PNTs and GO separately in the absence of the probe molecule at different electric fields from 10 – 60 V/mm. The Raman spectra recorded for FF-PNTs only (Fig. S17) revealed several characteristic FF-PNT bands (1001, 1031, 1583, and 1602 cm^{-1}). The amide III band (C–N stretching and N–H bending) is identified at 1250 cm^{-1}, whereas the amide I band (C=O stretching) is at 1688 cm^{-1}, in line with literature reports.[22] The overall intensity of FF-PNTs increased (~ 10^4) with applied electric field from 0 – 25 V/mm; however, the Raman intensity of FF-PNTs decreased with respect to peak-to-peak (with an increased background) ratio by ~ 10^2 with applied electric field from 0 – 25 V/mm, and increased when electric field values between ~ 30 – 60 V/mm were applied. Raman spectra of GO only at different electric fields were also recorded (Fig. S17b). Graphitic materials have typically been characterized by a highly dispersive band called the disorder-induced D-band (at 1350 cm^{-1}) and the graphitic mode (G-band) at higher wavenumbers (~ 1585 cm^{-1}).[1–4] According to a previous report, the observed position and the shape of this second-order G'-band obtained by 532-nm laser excitation corresponds to single-layer graphene.[31] The Raman intensity of GO increased ~ 10^3 with applied electric fields between 10 to 25 V/mm and then decreased as the electric field increased from 30 – 60 V/mm.

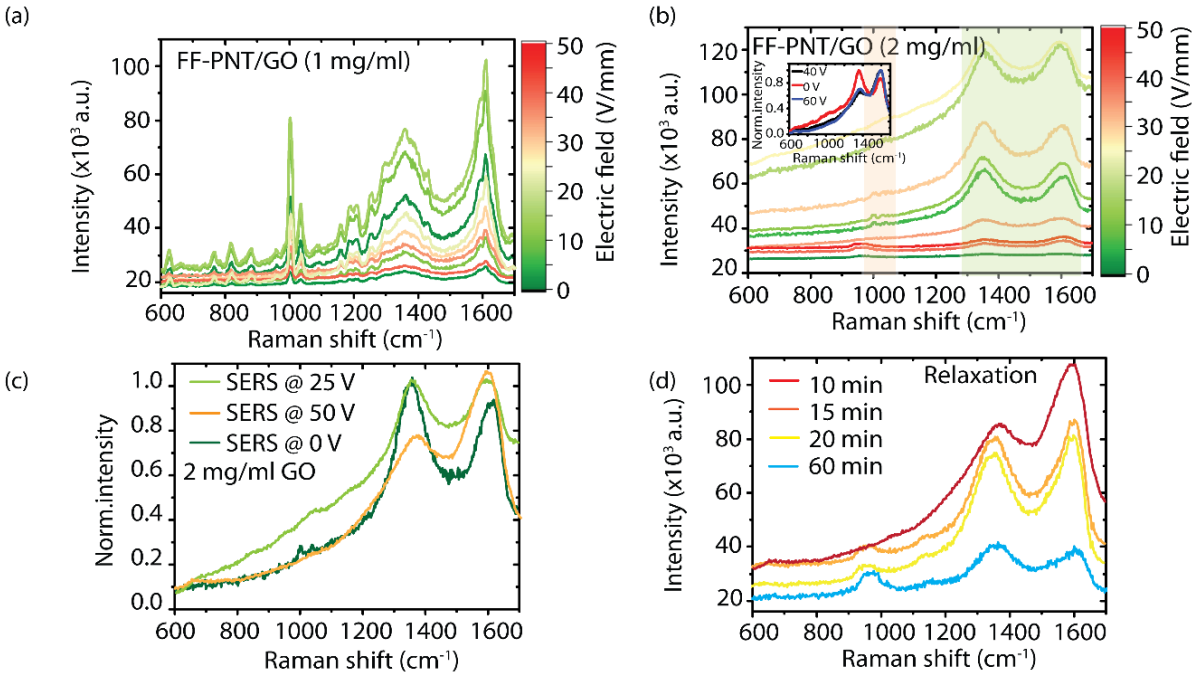

Figure S18. Raman spectra from FF-PNT/GO on Si in the absence of the probe molecule at applied electric fields from 0 – 50 or 60 V/mm at (a) 1 mg/ml GO with FF-PNTs and at (b) 2 mg/ml GO with FF-PNTs. The inset in (b) is the normalized spectrum at 0 V/mm versus 40 and 60 V/mm. (c) SERS spectra recorded at different electric fields and (d) the relaxation of the SERS signal intensity after the electric field is removed. The green shading in b corresponds to the main D- and G-bands of GO, while the orange shading refers to the breathing modes for FF-PNT at 1000 and 1003 cm^{-1}.

SERS measurements were then performed on the FF-PNT/GO template in the absence of the probe molecule. Templates prepared using a concentration of 1 mg/ml GO (Fig. S18a) resulted in the detection of Raman modes from both FF-PNT and GO, including bands at 1001, 1031, and 1250 cm^{-1} for FF-PNTs and 1350 and 1585 cm^{-1} for GO (D and G-band, respectively). The D-band at 1350 cm^{-1} and D'-band appearing as a shoulder of the G-band at 1620 cm^{-1} (Fig. S15) have been previously reported to be associated with impurities or surface charge.[1–4] In our case, the split and shift observed in the G-band when GO incorporates with FF-PNTs could be related to electric field-induced tuning of the Fermi level of GO. Previous studies have shown that the Fermi level of GO can be modulated continuously by the electric field and monitored through the Raman spectra.[23–25] The approach is based on modulating the energy alignment between the energy level of the molecule and the Fermi level of GO. Therefore, tuning the position of the Fermi level of metal using an external voltage source can, in principle, drive the entire system in and out of charge transfer resonance and could induce hole doping of GO, thereby decreasing the Fermi level of GO close to the LUMO of the probe molecule under study and increasing the contribution of the charge transfer mechanism enhancement. We propose that the enhanced Raman scattering of molecules discussed above on the FF-PNT/GO system is due to the charge transfer resonance mechanism, and the resonance conditions can be modulated by changing the Fermi level of GO.[23–25]

At a higher GO concentration (2 mg/ml), only G- and D-bands of GO can be seen at electric fields from 0 – 50 V/mm (Fig. S18b,c) from the FF-PNT/GO system. Weak FF-PNT Raman bands can be detected when the electric field increases from 30 – 60 V/mm and FF-PNT breathing modes assigned to the protein at 1001 and 1031 cm^{-1} can be seen. Relaxation of the SERS spectra intensity for the FF-PNT/GO system (with 2 mg/ml GO concentration) was observed (Fig. S18d). The original SERS signal intensity was recovered after 60 minutes, following removal of the electric field.

With increasing field strength, the spectra show that the D-band at 1350 cm^{-1} will start to decrease in intensity, whereas the G-band at 1585 cm^{-1} increases as the electric field increases to 25 V/mm (Fig. S18b,c). A shift in G-band position was also observed. Previous studies have shown that such an effect can be an indication of randomly distributed impurities or surface charges in the GO.[1–4, 26, 27] Electron accepting molecules (p-type doping) on GO have produced a similar effect with a reduction in the G-band (relative to the D-band).[28] This indicates a charge transfer process wherein GO donates electrons, which can result in an enhancement in fluorescence quenching efficiency, as observed from experiments with RhB and other dye molecules discussed above.

Stability of FF-PNT/GO template after the application of electric field

SEM images and dispersive X-Ray spectroscopy (EDX) mapping from templates after application of electric field are shown in Figs. S19 and S20, respectively.

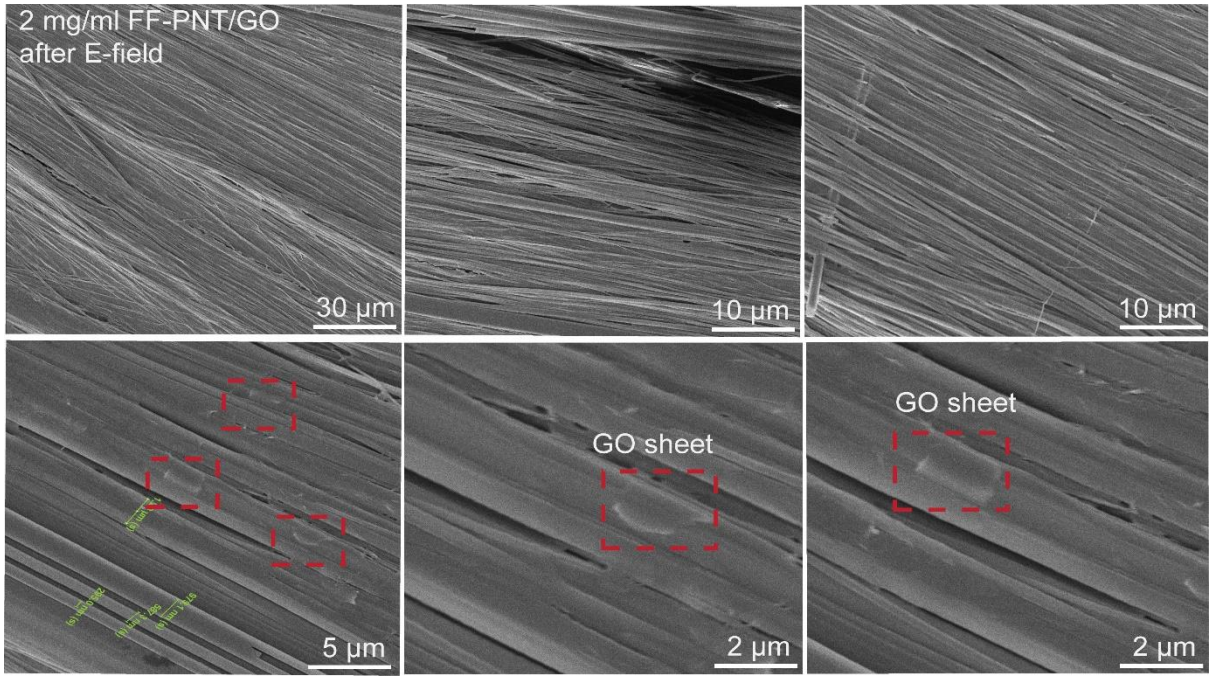

Figure S19. SEM images of the FF-PNT/GO template after the application of electric field from 5 to 60 V/mm indicating the stability of the composite structure.

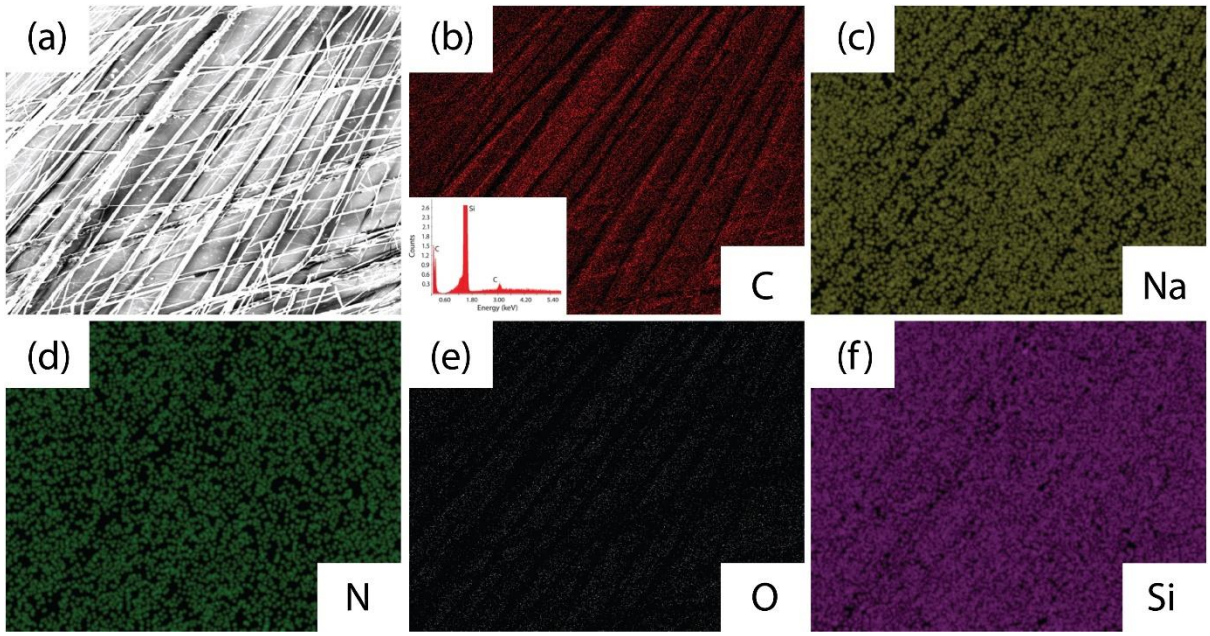

Figure S20. (a) SEM and (b-f) energy dispersive X-Ray spectroscopy (EDX) mapping of FF-PNT/GO composites showing the chemical composition of the template.

Biosensing studies

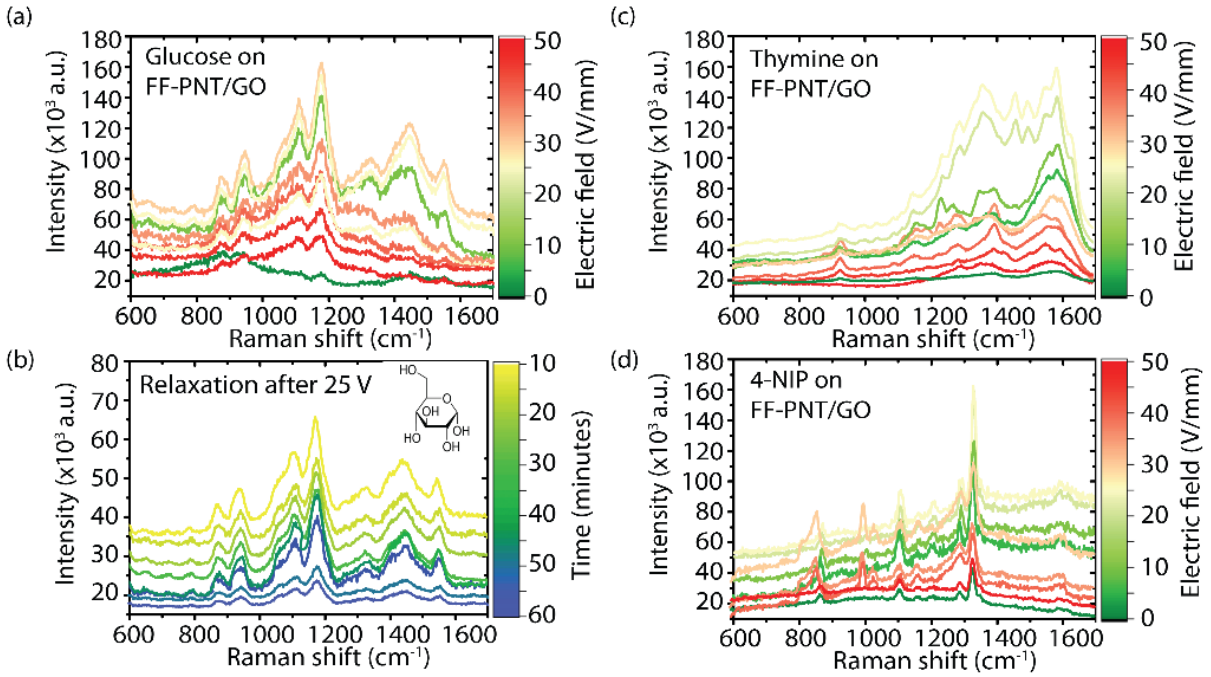

Figure S21. SERS spectra from glucose on FF-PNT/GO on Si recorded during the application of electric fields from 0 – 50 or 60 V/mm. (b) Relaxation over the course of ~ 60 minutes after removing the electric field. (b) SERS spectra from thymine recorded during the application of electric fields from 0 – 50 or 60 V/mm. (d) SERS spectra from 4-NIP probe molecules on FF-PNT/GO recorded during the application of electric fields from 0 – 50 or 60 V/mm. The inset in (c-d) shows a comparison of SERS spectra at 0 and 25 V/mm from thymine and 4-NIP, respectively.

SERS of thymine on FF-PNT/GO using a field of 10 – 25 V/mm (Fig. S21) showed significant increase in SERS signal intensity. With the appearance of thymine bands at 1600 cm^{-1}, 1520 cm^{-1} (C_2=O, C_4=O), 1477 cm^{-1} (CH_3), 1397 cm^{-1} (N_1–H, N_3–H), 1352 cm^{-1}, 1279 cm^{-1} (CH_3, C_6–H) 1221 cm^{-1} (C_5–C_9) , 1198 cm^{-1} (bend C_5–H, str C_5–C_6, C_6–N_1), 1351 cm^{-1} (CH_3), 1000 cm^{-1}, 935 cm^{-1} (N_1–H, N_3–H), in agreement with literature values.[29,30]

Interestingly, using thymine at a nanomolar concentration (Fig. S22) shows clear evidence of blinking with large variations in Raman peak intensities and positions over time. While these peaks differ in frequency, relative intensities, and line-width, they can all be assigned to vibrational bands of thymine as the average SERS signal is consistent with the Raman spectra of thymine at higher concentrations. This fluctuation is a strong indication of the sensitivity of the detection, which can be due to the interaction of FF-PNT with thymine through amine functional groups and the formation of hydrogen bonds. Previous studies have shown that fluctuation and blinking in Raman spectra is an indication of charge transfer in the system. Blinking observed on a FF-PNT/GO template with applied electric field was comparable to Raman blinking observed for noble metal-based SERS.[29,30] Raman enhancement and blinking was also observed for BSA and lysine on the FF-PNT/GO templates under an applied electric field (Fig. S23).

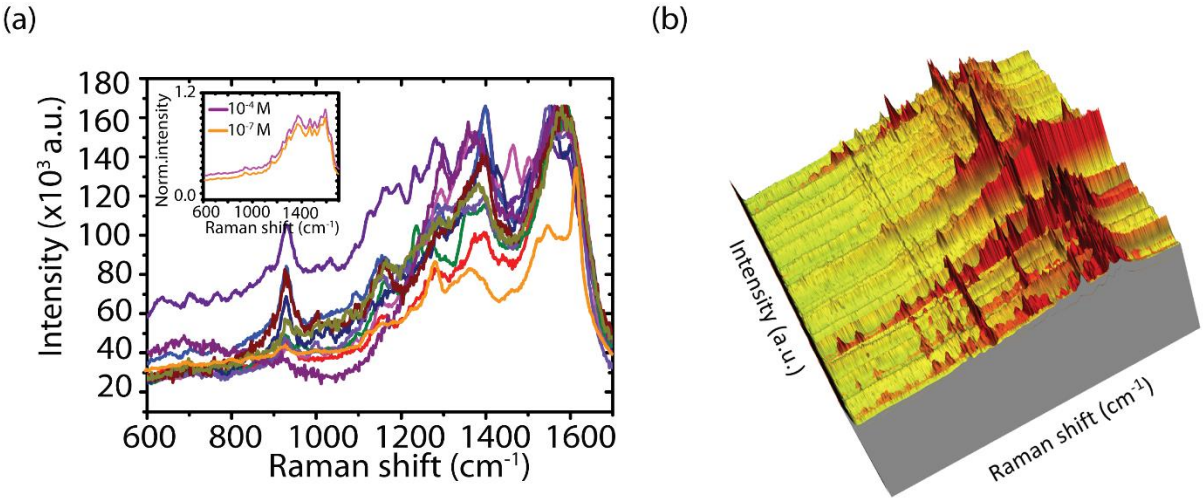

Figure S22. (a) Blinking from thymine on the FF-PNT/GO template with a 25 V/mm field. The inset in (a) shows the average SERS spectra of thymine on the template with applied electric field at high (purple) and low (orange) concentrations. (b) Blinking behavior as a function of time from thymine (0.09 µM) on the FF-PNT/GO template.

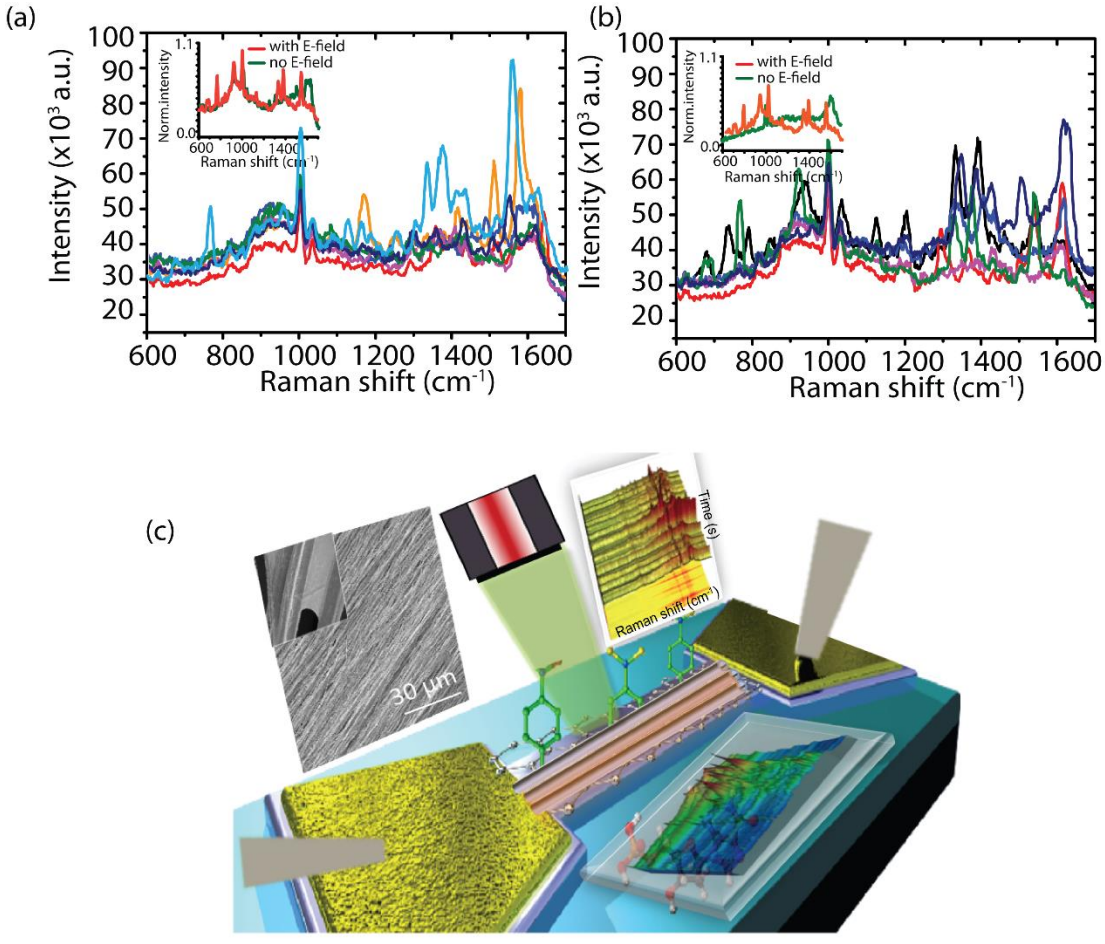

Figure S23. (a-b) Blinking from lys (0.09 µM) on FF-PNT/GO template with a 25 V/mm field. (c) Illustration of the device with FF-PNT/GO template. The inset in c (left) shows SEM images of the FF-PNT/GO template. The inset in c (right) shows blinking of the SERS signal from TMPyP as a function of time.

References

(1) Ivanov, M. S.; Khomchenko, V. A.; Salimian, M.; Kopyl, S.; Buryakov, A. M. Self-Assembled Diphenylalanine Peptide Microtubes Covered by Reduced Graphene Oxide / Spiky Nickel Nanocomposite : An Integrated Nanobiomaterial for Multifunctional Applications. *Materials & Design* **2018**, 142, 149–157.

(2) Yilmaz, M.; Babur, E.; Ozdemir, M.; Gieseking, R. L.; Dede, Y.; Tamer, U.; Schatz, G. C.; Facchetti, A.; Usta, H.; Demirel, G. Nanostructured Organic Semiconductor Films for Molecular Detection with Surface-Enhanced Raman Spectroscopy. *Nature Materials* **2017**, *16* (9), 918–924.

(3) Wang, Z.; Huang, P.; Bhirde, A.; Jin, A.; Ma, Y.; Niu, G.; Neamati, N.; Chen, X. A Nanoscale Graphene Oxide–Peptide Biosensor for Real-Time Specific Biomarker Detection on the Cell Surface. *Chemical Communications* **2012**, *48* (78), 9768.

(4) Li, Q.; Liu, L.; Zhang, S.; Xu, M.; Wang, X.; Wang, C.; Besenbacher, F.; Dong, M. Modulating Aβ33-42 Peptide Assembly by Graphene Oxide. *Chemistry - A European Journal* **2014**, *20* (24), 7236–7240.

(5) Almohammed, S.; Fedele, S.; Rodriguez, B. J.; Rice, J. H. Aligned Diphenylalanine Nanotube – Silver Nanoparticle Templates for High - Sensitivity Surface - Enhanced Raman Scattering. *Journal of Raman Spectoscopy* **2017**, *48,* 1799–1807.

(6) Almohammed, S.; Oladapo, S. O.; Ryan, K.; Kholkin, A. L.; Rice, J. H.; Rodriguez, B. J. Wettability Gradient-Induced Alignment of Peptide Nanotubes as Templates for Biosensing Applications. *RSC Adv.* **2016**, *6* (48), 41809–41815.

(7) Almohammed, S.; Zhang, F.; Rodriguez, B. J.; Rice, J. H. Photo-Induced Surface-Enhanced Raman Spectroscopy from a Diphenylalanine Peptide Nanotube-Metal Nanoparticle Template. *Scientific Reports* **2018**, *8* (1), 3880.

(8) Ryan, K.; Neumayer, S. M.; Maraka, H. V. R.; Kholkin, A. L.; Rice, J. H.; Rodriguez, B. J. Thermal and Aqueous Stability Improvement of Graphene Oxide Enhanced Diphenylalanine Nanocomposites. *Science and Technology of Advanced Materials* **2017**, *6996*, 1–25.

(9) Castillo, J.; Tanzi, S.; Dimaki, M.; Svendsen, W. Manipulation of Self-Assembly Amyloid Peptide Nanotubes by Dielectrophoresis. *Electrophoresis* **2008**, *29* (24), 5026–5032.

(10) Gong, Y.; Li, D.; Fu, Q.; Pan, C. Influence of Graphene Microstructures on Electrochemical Performance for Supercapacitors. *Progress in Natural Science: Materials International* **2015**, *25* (5), 379–385.

(11) Li, P.; Chen, X.; Yang, W. Graphene-Induced Self-Assembly of Peptides into Macroscopic-Scale Organized Nanowire Arrays for Electrochemical NADH Sensing. *Langmuir* **2013**, *29* (27), 8629–8635.

(12) Sil, S.; Kuhar, N.; Acharya, S.; Umapathy, S. Is Chemically Synthesized Graphene 'Really' a Unique Substrate for SERS and Fluorescence Quenching? *Scientific Reports* **2013**, *3* (1), 3336.

(13) Esin, A.; Baturin, I.; Nikitin, T.; Vasilev, S.; Salehli, F.; Shur, V. Y.; Kholkin, A. L. Pyroelectric Effect and Polarization Instability in Self-Assembled Diphenylalanine Microtubes. *Applied Physics Letters* **2016**, *109* (14), 1–5.

(14) Gan, Z.; Wu, X.; Zhu, X.; Shen, J. Light-Induced Ferroelectricity in Bioinspired Self-Assembled Diphenylalanine Nanotubes/Microtubes. *Angewandte Chemie - International Edition* **2013**, *52* (7), 2055–2059.

(15) Kholkin, A.; Amdursky, N.; Bdikin, I.; Gazit, E.; Rosenman, G. Strong Piezoelectricity in Bioinspired Peptide Nanotubes. *ACS Nano* **2010**, *4* (2), 610–614.

(16) Andrade-Filho, T.; Ferreira, F. F.; Alves, W. A.; Rocha, A. R. The Effects of Water Molecules on the Electronic and Structural Properties of Peptide Nanotubes. *Physical Chemistry Chemical Physics* **2013**, *15* (20), 7555.
(17) de Abajo, F. J. G. Graphene Plasmonics: Challenges and Opportunities. *ACS Photonics* **2014**, *1 (3)*, 135–152.
(18) Goul, R.; Das, S.; Liu, Q.; Xin, M.; Lu, R.; Hui, R.; Wu, J. Z. Quantitative Analysis of Surface Enhanced Raman Spectroscopy of Rhodamine 6G Using a Composite Graphene and Plasmonic Au Nanoparticle Substrate. *Carbon* **2017**, *111*, 386–392.
(19) Lu, R.; Konzelmann, A.; Xu, F.; Gong, Y.; Liu, J.; Liu, Q.; Xin, M.; Hui, R.; Wu, J. Z. High Sensitivity Surface Enhanced Raman Spectroscopy of R6G on in Situ Fabricated Au Nanoparticle/Graphene Plasmonic Substrates. *Carbon* **2015**, *86*, 78–85.
(20) Osawa, M.; Matsuda, N.; Yoshii, K.; Uchida, I. Charge Transfer Resonance Raman Process in Surface-Enhanced Raman Scattering from p-Aminothiophenol Adsorbed on Silver: Herzberg-Teller Contribution. *Journal of Physical Chemistry* **1994**, *98* (48), 12702–12707.
(21) Kim, K.; Lee, S. H.; Kim, K. L.; Shin, K. S. Visible Light Response of Silver 4-Aminobenzenethiolate and Silver 4-Dimethylaminobenzenethiolate Probed by Raman Scattering Spectroscopy. *Journal of Raman Spectroscopy* **2013**, *44* (4), 518–524.
(22) Wu, X.; Xiong, S.; Wang, M.; Shen, J.; Chu, P. K. Low-Frequency Raman Scattering of Bioinspired Self-Assembled Diphenylalanine Nanotubes/Microtubes. *Optics Express* **2012**, *20* (5), 5119–5126.
(23) Xu, H.; Xie, L.; Zhang, H.; Zhang, J. Effect of Graphene Fermi Level on the Raman Scattering Intensity of Molecules on Graphene. *ACS Nano* **2011**, 5, 5338–5344.
(24) Yu, Y.-J.; Zhao, Y.; Ryu, S.; Brus, L. E.; Kim, K. S.; Kim, P. Tuning the Graphene Work Function by Electric Field Effect. Supplementary Information. *Nano Letters* **2009**, *9* (10), 3430–3434.
(25) Balu, R.; Zhong, X.; Pandey, R.; Karna, S. P. Effect of Electric Field on the Band Structure of Graphene/Boron Nitride and Boron Nitride/Boron Nitride Bilayers. *Applied Physics Letters* **2012**, *100* (5), 1–4.
(26) Liu, J.; Li, Q.; Zou, Y.; Qian, Q.; Jin, Y.; Li, G.; Jiang, K.; Fan, S. The Dependence of Graphene Raman D-Band on Carrier Density. *Nano Letters* **2013**, *13* (12), 6170–6175.
(27) Iqbal, M. W.; Iqbal, M. Z.; Khan, M. F.; Jin, X.; Hwang, C.; Eom, J. Modification of the Structural and Electrical Properties of Graphene Layers by Pt Adsorbates. *Science and Technology of Advanced Materials* **2014**, *15*, 055002.
(28) Late, D. J.; Ghosh, A.; Chakraborty, B.; Sood, A. K.; Waghmare, U. V.; Rao, C. N. R. Molecular Charge-Transfer Interaction with Single-Layer Graphene. *Journal of Experimental Nanoscience* **2011**, *6* (6), 641–651.
(29) Madzharova, F.; Heiner, Z.; Guhlke, M.; Kneipp, J. Surface-Enhanced Hyper-Raman Spectra of Adenine, Guanine, Cytosine, Thymine, and Uracil. *Journal of Physical Chemistry C* **2016**, *120* (28), 15415–15423.
(30) Ten, G. N.; Burova, T. G.; Baranov, V. I. Calculation and Analysis of Vibrational Spectra of Adenine – Thymine , Guanine – Cytosine , and Adenine – Uracil Complementary Pairs in the Condensed State. *Journal of Applied Spectroscopy* **2009**, *76* (1), 84–92.